

HST/ACS IMAGING OF OMEGA CENTAURI: OPTICAL COUNTERPARTS OF CHANDRA X-RAY SOURCES

ADRIENNE M. COOL,¹ DARYL HAGGARD,^{2,3} TERSI ARIAS,^{1,4} MICHELLE BROCHMANN,^{1,5} JASON DORFMAN,^{1,6} APRIL GAFFORD,^{1,7} VIVIAN WHITE,^{1,8} AND JAY ANDERSON⁹

(Received September 14, 2012; Accepted December 8, 2012)
Draft version November 4, 2018

ABSTRACT

We present results of a search for optical counterparts of X-ray sources in and toward the globular cluster Omega Centauri (NGC 5139) using the Advanced Camera for Surveys (ACS) on the *Hubble Space Telescope*. The ACS data consist of a mosaic of Wide Field Channel (WFC) images obtained using F625W, F435W, and F658N filters; with 9 pointings we cover the central $\sim 10' \times 10'$ of the cluster and encompass 109 known *Chandra* sources. We find promising optical counterparts for 59 of the sources, ~ 40 of which are likely to be associated with the cluster. These include 27 candidate cataclysmic variables (CVs), 24 of which are reported here for the first time. Fourteen of the CV candidates are very faint, with absolute magnitudes in the range $M_{625} = 10.4 - 12.6$, making them comparable in brightness to field CVs near the period minimum discovered in the SDSS (Gänsicke et al. 2009). Additional optical counterparts include three BY Dra candidates, a possible blue straggler, and a previously-reported quiescent low-mass X-ray binary (Haggard et al. 2004). We also identify three foreground stars and 11 probable active galactic nuclei. Finally, we report the discovery of a group of seven stars whose X-ray properties are suggestive of magnetically active binaries, and whose optical counterparts lie on or very near the metal-rich anomalous giant and subgiant branches in ω Cen. If the apparent association between these seven stars and the RGB/SGB-a stars is real, then the frequency of X-ray sources in this metal-rich population is enhanced by a factor of at least five relative to the other giant and subgiant populations in the cluster. If these stars are not members of the metal-rich population, then they bring to 20 the total number of red stragglers (also known as sub-subgiants) that have been identified in ω Cen, the largest number yet known in any globular cluster.

Keywords: globular clusters: individual (NGC 5139) — binaries: close — cataclysmic variables — color-magnitude diagrams (HR diagram) — white dwarfs — X-rays: binaries

1. INTRODUCTION

As the most massive globular cluster in the Milky Way, and the first to reveal the presence of multiple stellar populations, ω Cen has garnered significant attention from observers and theorists alike (e.g., Cannon & Stobie 1973, Freeman & Rodgers 1975, Norris & Da Costa 1995, Norris, Freeman, & Mighell 1996, Suntzeff & Kraft 1996, van Leeuwen, Hughes, & Piotto 2002). Detailed studies of its stellar populations reveal a remarkable and unexpected complexity, beginning with the discovery of an anomalous red giant branch (Lee et al. 1999, Pancino et al. 2000) with metallicity ten times that of the ma-

jority population of giants in the cluster (Pancino et al. 2000, Sollima et al. 2005, Johnson & Pilachowski 2010). Since then, it has also been shown to harbor a double main sequence (Anderson 1997, 2002a, 2003; Bedin et al. 2004), and a multiplicity of subgiant branches (Ferraro et al. 2004; Villanova et al. 2007). A large helium enhancement, possibly caused by early self-enrichment from AGB stars (Renzini 2008, D'Ercole et al. 2008), has been invoked (Norris 2004, King et al. 2012) to explain the startling finding that the redder of the primary main-sequence populations is the more metal-poor of the two (Piotto et al. 2005). There is considerable debate as to whether ω Cen is a globular cluster at all. Growing evidence points instead to its being the stripped remnant of a dwarf galaxy accreted by the Milky Way (Norris et al. 1996, Lee et al. 1999, Bekki & Freeman 2003, Renzini 2008).

A complete picture of the stellar populations in a globular cluster includes its binary stars. Like single stars, binaries can provide insight into the conditions of a cluster's formation. Knowledge of binary populations is also central to an understanding of cluster dynamical evolution (see, e.g., Hut et al. 1992). With a half-mass relaxation time approaching the Hubble time, and a moderate central density of $\sim 1500 L_{\odot}/\text{pc}^3$ (Djorgovski 1993), many of ω Cen's primordial binaries are likely to have survived to the present day (Davies 1997, Ivanova et al. 2006). At the same time, its unusually large core ($r_c \simeq 3.7$ pc) is such that significant numbers of stellar colli-

¹ Department of Physics and Astronomy, San Francisco State University, 1600 Holloway Ave., San Francisco, CA 94132, USA; cool@sfsu.edu

² Center for Interdisciplinary Exploration and Research in Astrophysics, Physics and Astronomy Department, Northwestern University, 2145 Sheridan Road, Evanston, IL 60208, USA; dhaggard@northwestern.edu

³ CIERA Postdoctoral Fellow

⁴ Dept. of Atmospheric and Oceanic Sciences, UCLA, Los Angeles, CA 90095, USA

⁵ Department of Physics, University of Washington, Seattle, WA 98195, USA

⁶ Bays Mountain Park & Planetarium, Kingsport, TN 37660, USA

⁷ JATO Aviation, San Carlos, CA, 94070, USA

⁸ Astronomical Society of the Pacific, San Francisco, CA 94112, USA

⁹ Space Telescope Science Institute, Baltimore, MD 21218, USA

sions and near misses are expected to have occurred over its lifetime (Verbunt & Meylan 1988, Di Stefano & Rappaport 1994). Regardless of its origins, the sheer number of binaries that ω Cen is likely to harbor by virtue of its enormous mass ($\sim 3 \times 10^6 M_{\odot}$; Meylan 2002) provides an opportunity to observe large numbers of binaries all at essentially the same distance, and to uncover potentially rare classes of systems.

One fruitful way to search for binary stars in globular clusters is via X-ray imaging. At the limiting luminosities reached in nearby globular clusters with the *Chandra X-ray Observatory*, a diverse array of binaries can be revealed. Beyond the high-luminosity globular cluster sources known since the early days of X-ray astronomy (Giacconi et al. 1974) and understood to be accreting neutron stars (Clark 1975), the much more abundant low-luminosity X-ray sources include cataclysmic variables (CVs; Hertz & Grindlay 1983a), quiescent low-mass X-ray binaries (qLMXBs; Verbunt, van Paradijs, & Elson 1984), millisecond pulsars (MSPs; e.g., Grindlay et al. 2002) and chromospherically active stars. The latter may be the result of enhanced coronal activity due to tidal locking in a binary system; hereafter we shall use the term “active binary” (AB) to refer to either the main-sequence variety (BY Dra stars—Dempsey et al. 1997) or the subgiant variety (RS CVn stars—Dempsey et al. 1993), both of which have been seen in globular clusters (e.g., Kaluzny et al. 1996, Taylor et al. 2001, Albrow et al. 2001). Among the low-luminosity sources, only the qLMXBs (also known as quiescent neutron stars, or qNS), with their distinctive soft X-ray spectra and moderate luminosities, can be identified on the basis of X-ray observations alone (Brown, Bildsten, & Rutledge 1998, Rutledge et al. 2000). For others, optical (or radio, in the case of MSPs) follow-up is essential. In the optical, the resolving power of the *Hubble Space Telescope* (*HST*) is crucial; the vast majority of CVs now known in globulars are hopelessly lost in the light of brighter neighbors in ground-based imaging.

Early X-ray imaging of ω Cen with Einstein IPC revealed multiple low-luminosity X-ray sources in and toward the cluster (Hertz & Grindlay 1983b). The source closest to the cluster center, IPC source C, was subsequently resolved into three separate sources with ROSAT HRI (Verbunt & Johnston 2000). Using the HRI positions, Carson, Cool, & Grindlay (2000) identified two of these as probable CVs based on the discovery of $H\alpha$ -bright, UV-bright optical counterparts in *HST*/WFPC2 imaging. IPC source B, $\sim 4'$ from the cluster center, coincides with a *Chandra* source subsequently identified as a qNS (Rutledge et al. 2002, Haggard et al. 2004). Two other sources (“A” and “D”), both more than $10'$ from the cluster center, were shown to be foreground dMe stars (Cool et al. 1995a). Gendre et al. (2003) increased to 27 the total number of X-ray sources known within the half-mass radius of ω Cen using *XMM-Newton*, and found that their X-ray properties are consistent with their being a combination of CVs and active binaries. More recently, a 69 ksec ACIS-I exposure with *Chandra* that reached a limiting luminosity of $L_x \sim 10^{30}$ erg s $^{-1}$ revealed 180 X-ray sources in and toward the cluster, 81 within the half-mass radius (Haggard, Cool, & Davies 2009, hereafter HCD09).

One of the challenges in identifying binary stars in

ω Cen using X-ray imaging is its large angular size on the sky. Owing to this, we expect a significant fraction of the *Chandra* sources to be active galaxies behind the cluster (AGN; see HCD09 for a detailed discussion). With the exception of the qNS, no unique X-ray spectral signature allows us to distinguish probable AGN from accreting binaries in the cluster, particularly given the faintness of the sources. To determine which of these sources are binaries within the cluster, we must therefore search for optical counterparts for all the X-ray sources present, with the expectation that only a fraction are likely to be associated with the cluster.

Here we report the results of a search for optical counterparts of *Chandra* sources using *HST*’s Advanced Camera for Surveys (ACS). Preliminary results of this study were reported by Haggard et al. (2010). The ACS/WFC data consist of a mosaic of 3×3 pointings which encompasses 109 of the *Chandra* sources. We use the $H\alpha$ imaging technique that has been applied successfully to searches for CVs in other clusters (e.g., Cool et al. 1995b, Grindlay et al. 1995, Bailyn et al. 1996, Pooley et al. 2002, Anderson, Cool, & King 2003, Cohn et al. 2010). This method is also sensitive to qLMXBs which, like CVs, are characterized by strong hydrogen emission lines. Using these data, an optical counterpart for the source initially identified as a qNS on the basis of its X-ray spectrum alone (Rutledge et al. 2002) was reported by Haggard et al. (2004). While chromospherically active binaries have rather weak emission lines compared to accreting binaries (e.g., Chevalier & Ilovaisky 1997), the subset with the greatest coronal activity can also be identified using this $H\alpha$ imaging technique (e.g., Taylor et al. 2001, Cohn et al. 2010).

The outline of the paper is as follows. In Section 2 we describe the observations, together with the astrometric and photometric techniques used to analyze the data. We then describe in detail the method by which we evaluated potential optical counterparts. In Section 3 we present the most promising optical counterpart identifications, dividing them into categories based on their locations in $B_{435} - R_{625}$ vs. R_{625} and $H\alpha - R_{625}$ vs. R_{625} color-magnitude diagrams (CMDs). We discuss the results in Section 4 and summarize them in Section 5.

2. OBSERVATIONS AND ANALYSIS

We obtained images of ω Cen with the Wide Field Channel (WFC) of the Advanced Camera for Surveys (ACS) on *HST* using F625W (R_{625}), F435W (B_{435}), and F658N ($H\alpha$) filters on 2002 June 27 – 30. The observations consist of a 3×3 mosaic covering $\sim 10' \times 10'$ approximately centered on the cluster center (Fig. 1). The full mosaic extends beyond the cluster’s half mass radius of $\sim 4.2'$ (Harris 1996) and encompasses 109 of the 180 X-ray sources we detected in *Chandra* observations of ω Cen (HCD09).

At each of the 9 tiles in the mosaic, we obtained a total of 12 exposures: 4×440 s with the $H\alpha$ filter (F658N), 3×340 s with each of the broad-band filters (F625W and F435W), and one short exposure in each of the broad-band filters (8s and 12s in F625W and F435W, respectively). A gain of 2 electrons/DN was adopted so as to make full use of the $\sim 85,000$ electron well-depth of the WFC CCDs. Shifts of $\sim 5''$ were made between each of the 4 $H\alpha$ exposures. In the two broad-band filters,

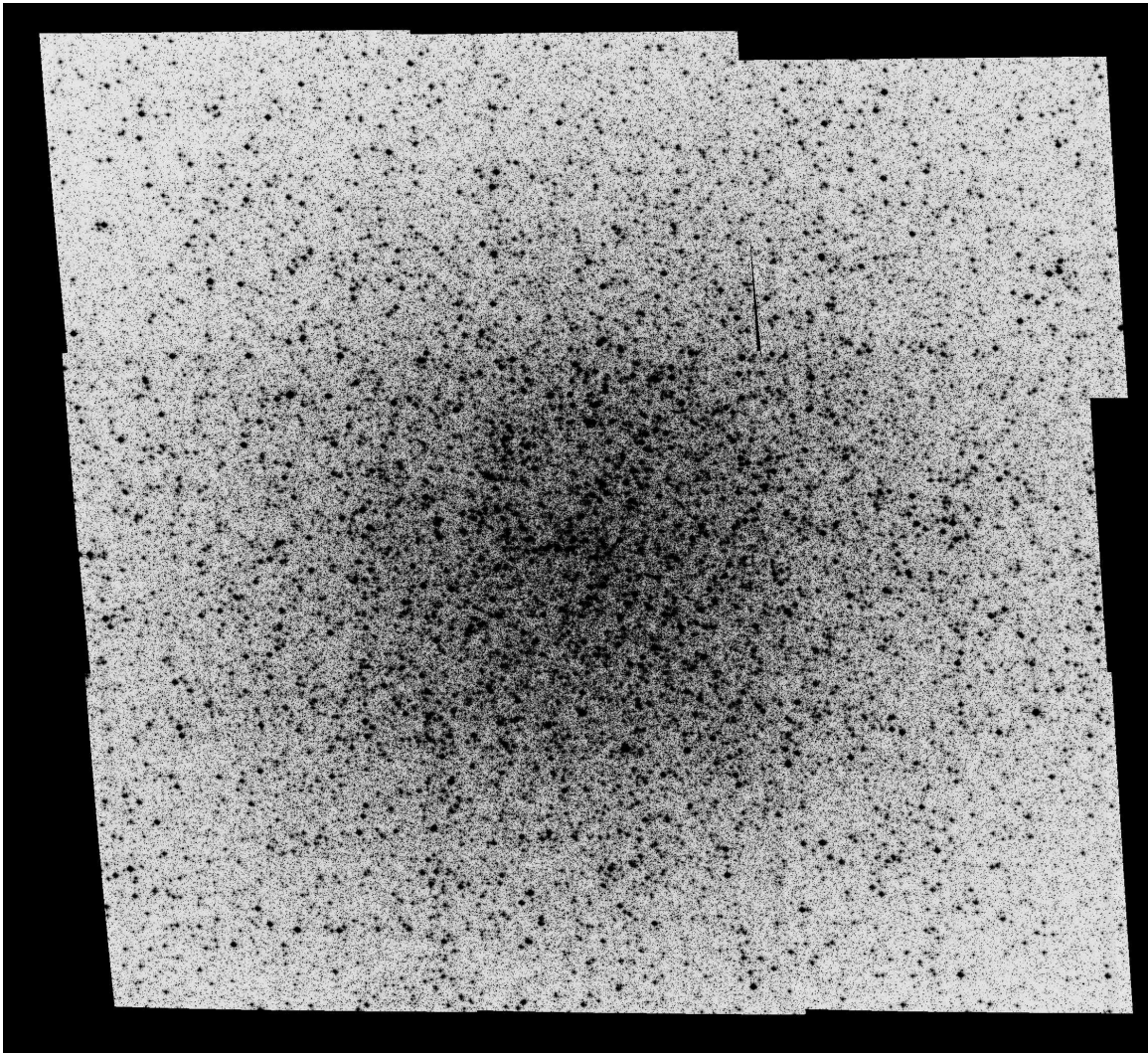


Figure 1. Mosaic of ω Cen constructed from ACS/WFC B_{435} images at nine different pointings. Note that the northwest tile was slightly offset from the planned pointing, apparently due to the misacquisition of guide stars. The field of view is approximately $10' \times 10'$; north is up and east is to the left.

shifts of $7''.5$ were adopted so that the 3 available exposures span the same region as the $H\alpha$ exposures. These “dither” patterns insure that any given star in the mosaic lands in the $\sim 2''.5$ -wide chip gap at most once in any filter. With a minimum of 3 long exposures in each filter we are also able to identify cosmic rays reliably.

2.1. Astrometry

To map the positions of *Chandra* sources onto the ACS/WFC images, we first applied a distortion correction to the individual WFC images using the solution obtained for the F475W filter from a study of 47 Tuc (Anderson 2002b). The internal accuracy of this solution should be ~ 0.15 WFC pixel ($\simeq 0''.0075$). We then stitched together all the individual B_{435} frames to make a mosaic of the entire field in that filter. The images fit together well, with no sign of misaligned star images where chips overlap, indicating that the distortion correction was working well.

To determine the R.A. and Dec. associated with stars on the mosaic, we used the star lists of Kaluzny et al. (1996) and van Leeuwen et al. (2000). More than 15,000 of the former and 4000 of the latter fall within the field

of view of our mosaic. There is a small zeropoint offset of $0''.5$ between the two systems, which we take to be indicative of the uncertainty in the absolute frame; we used the Kaluzny system to define the transformation between our mosaic system and R.A. and Dec. We estimate that, at any given location in the mosaic, the absolute astrometry should be accurate to $\lesssim 0''.2$ due to uncertainties in stitching together the individual images.

In our search for optical counterparts we initially adopted $1''.0$ error circles. This radius was chosen in consideration of the $0''.6$ uncertainty (90% confidence) in *Chandra*’s absolute coordinate system, uncertainties in *wavdetect* positions at the level of $\sim 0''.5$ several arcminutes off-axis (Feigelson et al. 2002), and the $\lesssim 0''.2$ uncertainties in our mosaic construction. As a check on whether this error budget was sufficiently generous, we recovered the two stars identified by Carson et al. (2000) as probable CVs; both are $< 0''.3$ from their nominal positions. The optical counterpart to the qNS identified by Haggard et al. (2004), $4''.4$ from the cluster center, is $< 0''.5$ from the nominal position and thus also well within the $1''$ circle.

After we had analyzed roughly one third of the sources

we computed a boresight correction using 14 promising optical counterparts identified as of then, including the 4 objects found in our previous studies of ω Cen (Carson et al. 2000, Haggard et al. 2004). The original error circle was centered at pixel coordinate (200.5, 200.5) on the 401×401 pixel “patches” that we extracted surrounding each X-ray source (see §2.2) and had a radius of 20 pixels ($1''.0$). The boresight-corrected error circle is centered at (206.1, 206.6). The standard deviation of the offsets between the observed positions of these 14 optical counterparts and this new center was ~ 4 pixels in both x and y . Based on this, we chose a 12 pixel ($0''.6$) radius ($\sim 3\sigma$) for the new error circle.¹⁰ This new circle lies almost entirely within the larger $1''$ circle (see Fig. 4), but has an area only 0.36 times as large (see also §2.3). For simplicity we have adopted the same size error circle for all sources; we verify below (see §3.2) that it is sufficiently generous even for faint X-ray sources for which the uncertainty in the X-ray position dominates the error budget. The full set of optical identifications appears in Table 1.

2.2. Photometry

We began with “flt” images that had been processed through the standard *HST* calibration pipeline, including debiasing, dark subtraction, and flat-field correction, using the best available calibration images as of 2004 August 05. We then used the data quality files to identify saturated pixels in each image and set them to a high value (99000) so that they would be easily recognizable in the subsequent analysis. We extracted 401×401 pixel ($\sim 20'' \times 20''$) “patches” around each of the *Chandra* source positions (HCD09) in each of the images.¹¹ For 95 of the 109 sources, the result is a set of 12 small images to be analyzed, with the source position close to the center of each. For 13 of the sources, the fact that the tiles of the mosaic overlap one another meant that images were available from more than one tile. In these cases, we analyzed images from the tile with the most images, which was a full set of 12 in all but two cases (24d with 9 images, and 24f with 8 images). One source (31d) falls near a small gap created by the slightly mis-pointed tile (see Fig. 1), but still has coverage in 9 images.

Despite the high resolution of the ACS/WFC ($0''.05$ pixels), the images are still quite crowded, with many stars overlapping one another. We therefore chose to use DAOPHOT and ALLSTAR (Stetson 1987) for the analysis. We also found that DAOPHOT/ALLFRAME (Stetson 1994), with its capacity to analyze multiple images simultaneously and require consistent positions for all stars, was very valuable given the level of crowding and numerous cosmic rays in the images. The two labor-intensive parts of the analysis are the creation of high-quality point-spread functions (PSFs) and the production of reliable and complete star lists in the region of the X-ray source error circles. Because of the possibility that an interesting optical counterpart could be missed in any fully automated process, we decided to take a more hands-on approach. We describe each of these steps in

detail below.

We began by creating PSFs empirically for each individual long exposure of each patch. For the short R_{625} and B_{435} exposures, the PSF from the long exposure at the corresponding dithers were adopted. Our earlier tests on the patch containing the qLMXB (Haggard et al. 2004) had shown that separate PSFs for each exposure produced the best results. We found that, when analyzing these small image patches, constant PSFs worked well. Typically $\sim 10 - 40$ of the most isolated stars were used to define the PSF in each case, including a few saturated stars to help to better define the model at large radii. PSF radii of 7 – 11 pixels were adopted, with the smaller radii generally being required in the most crowded patches. These PSF sizes were adequate to model and remove most stars in the X-ray error circles very well. We iterated the PSF-creation process as many times as needed, removing neighbor stars, checking the quality of subtractions, and removing and/or adding more PSF stars as needed.

After extensive experimentation with DAOPHOT and PSF-fitting techniques on the WFC “flt” images, we found that pixels adjacent to saturated pixels were also affected by saturation. This became apparent when we found that the measured magnitudes of saturated stars in long exposures were systematically brighter than those obtained from the short exposures. We therefore decided to flag all pixels adjacent to saturated pixels and ignore them in both the creation of PSFs and the generation of magnitudes. This eliminated the systematic bias in the measurement of saturated stars. The quality of PSFs also improved substantially, allowing us to make much better use of saturated stars to determine PSF structures at large radii.

Initial star lists were obtained using automated DAOPHOT/FIND on one of the R_{625} images. For each patch, we then examined by eye the region surrounding the *Chandra* source position at the center of the patch. We focused initially on a $1''$ error circle surrounding the nominal X-ray source position, and later narrowed our search to a $0''.6$ circle once the boresight correction had been applied (see §2.1). We began by removing from the list any objects that were clearly cosmic rays or other artifacts, which we determined by blinking the different images against one another. We also adopted a conservative approach and removed any objects that we were not confident were real (e.g., in regions where multiple stars overlapped). We then ran ALLSTAR and ALLFRAME and carefully examined the subtracted images. Remaining objects that appeared consistently in all 3 subtracted R_{625} and/or B_{435} images were then added to the star list by hand. This procedure was repeated until no additional objects could be seen in the subtracted images. Typically 3 to 5 iterations were needed to produce the final list of stars. This work was done primarily using the 3 long R_{625} exposures, which include the faintest stars. We also examined the $H\alpha$ and long B_{435} exposures to check for any additional very blue or $H\alpha$ -bright objects.

When the PSFs and star lists were finalized we ran ALLSTAR and ALLFRAME one last time to generate final positions and magnitudes for all the stars. We then matched stars up across the 12 frames, requiring that a star be found in at least 4 of the frames for it to be included in the final list. We retained both ALLSTAR and

¹⁰ For a bivariate normal distribution, this is equivalent to a 99% error circle.

¹¹ Patch images may be found at <http://www.physics.sfsu.edu/~cool/omegaCen/>.

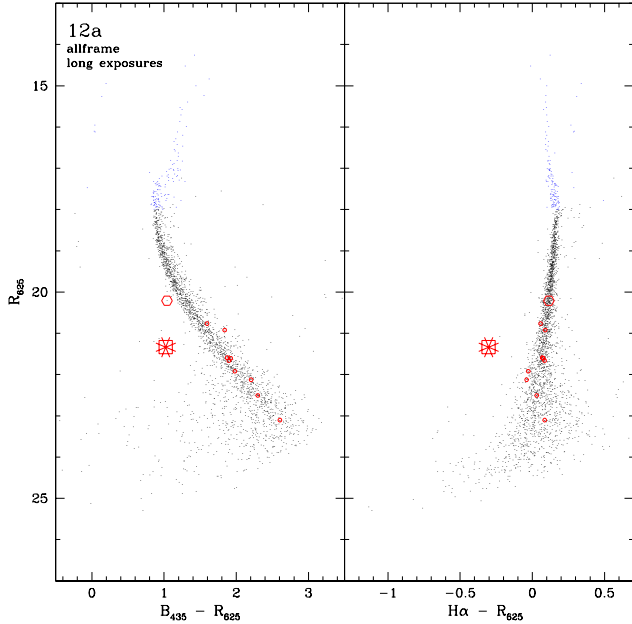


Figure 2. $B_{435} - R_{625}$ and $H\alpha - R_{625}$ color-magnitude diagrams for stars in the vicinity of *Chandra* X-ray source 12a. Small dots are all stars in a $20'' \times 20''$ patch surrounding the source position (saturated stars in blue, non-saturated stars in black). Stars that lie inside the $0.6''$ error circle that was scrutinized in detail are marked with open red circles. Small red circles are stars that lie on the main sequence or SGB or RGB in both the $B_{435} - R_{625}$ vs. R_{625} and $H\alpha - R_{625}$ vs. R_{625} CMDs. Larger symbols are used to indicate objects that lie off these sequences in one or both diagrams. Symbol shapes indicate the quality of the candidates (see §2.4). An asterisk marks the object most likely to be the optical counterpart of the X-ray source. In this case it is an object that is both blue and $H\alpha$ -bright: a probable cataclysmic variable (see §3.1).

ALLFRAME results because, in a few cases, the distortion of the ACS/WFC was sufficiently large (e.g., when a source lands near an edge in one dither) that the subtracted images in ALLFRAME show evidence of imperfect star positions. In these cases we carefully assessed whether ALLSTAR or ALLFRAME gave more reliable results by examining subtracted images and the width of the main sequence in color-magnitude diagrams (CMDs). In the one case (21c) where the ALLSTAR results were deemed more reliable (and a candidate optical counterpart was found), we report these results in Fig. 3 and Table 1. We transformed our instrumental magnitudes to the VEGAMAG system using the zeropoints and aperture corrections provided by Sirianni et al. (2005) for the ACS/WFC.

2.3. Candidate Inspection

Once we had constructed CMDs for each patch, we carried out a systematic evaluation of all potentially interesting objects. All objects that did not lie on or very near the main sequence or giant branch in both the $B_{435} - R_{625}$ and $H\alpha - R_{625}$ CMDs were evaluated for reliability of the photometry. We did this by examining the object in all the individual images to check the potential impact of near neighbors, cosmic rays, and diffraction spikes, and by looking at how cleanly DAOPHOT removed it from each of the images. We also took account of the consistency of the multiple independent measurements in the

different filters. During this part of the analysis we carefully examined all the subtracted images to look for signs that any of the objects were extended (i.e., whether flux was left behind after a point source was subtracted), and for additional objects that might have been missed in previous rounds. When additional objects were found, we added them to the list and remade the CMDs before further evaluation.

Based on these considerations, objects of potential interest were classified as having one of four “qualities,” 0 through 3. Objects for which no potential problems were found, such that their positions in the CMDs are very reliable, were classified as having quality 0. Objects for which only relatively minor problems were present, such that their positions in the CMDs should still be reliable, were classified as quality 1. Objects for which potentially significant problems were found, such that their positions in the CMD might not be reliable, were classified as quality 2. Objects that were apparently real stars, but for which significant problems were found (e.g. diffraction spike, much brighter neighbor very close by, etc.), such that their positions in the CMDs are unlikely to be reliable, were classified as quality 3. Here it should be made clear that the quality flag is an assessment of the reliability of an object’s measured position within the CMDs (i.e., whether the object can be reliably said to be on or away from the nearest well-populated sequence), not of the probability of its being the actual optical counterpart of the X-ray source.

As an example, we show in Figure 2 the CMDs for the patch corresponding to the northernmost of the three bright X-ray sources in the core (*Chandra* source 12a, HCD09), referred to by Carson et al. (2000) as XC. The small dots in the image are all stars within the $\sim 20'' \times 20''$ patch; these include many artifacts and poorly measured stars since no effort was made to “clean” the area of the patch outside the X-ray error circle. Small circles represent stars that lie within the $0.6''$ error circle; these objects should all be real, as they were carefully assessed by eye. Larger symbols are used to represent those objects that were scrutinized for photometric reliability; different symbols are used to represent different qualities (triangle, square, pentagon and hexagon for quality 0, 1, 2, and 3, respectively). In this particular patch, 11 objects landed inside the error circle. Two lie off the main sequence in one or both CMDs and were assessed for reliability. Of these, one was deemed likely to be reliable (the square) while the other was deemed likely not to be (the hexagon). Finally, we added an asterisk to the object that we deemed most likely to represent the optical counterpart of the X-ray source. Only quality 0 and 1 objects were considered as potential counterparts. In this patch there was one such object. It is both blue and $H\alpha$ -bright; we show below (see §3.1) that it is likely to be a cataclysmic variable, a classification supported by previous work (HCD09 and references therein).

In Fig. 3 we present CMDs like those in Fig. 2 for the 59 patches in which one or more quality 0 or 1 object was found to lie off the main sequence in one or both diagrams ($B_{435} - R_{625}$ vs. R_{625} and/or $H\alpha - R_{625}$ vs. R_{625}).¹² Each pair of panels corresponds to one X-ray source, with the

¹² Larger versions of these CMDs may be found at <http://www.physics.sfsu.edu/~cool/omegaCen/>.

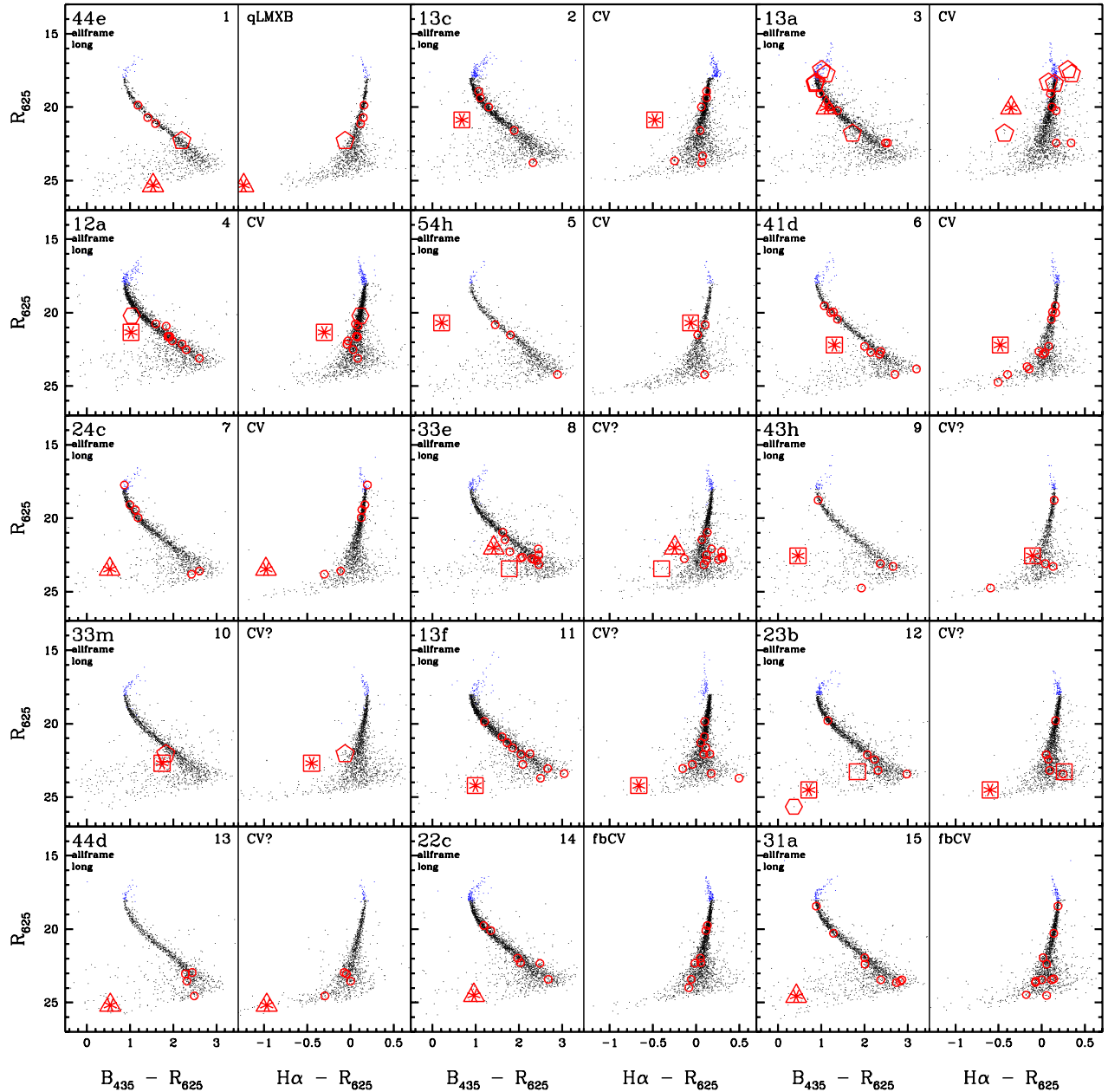


Figure 3. Full set of 59 CMD pairs; symbols as in Fig. 2.

name of the source from HCD09 listed in the upper left corner of the left panel. For ease of comparing related candidates to one another, CMDs are grouped according to the classification of the candidate (see §3) and sorted in order of R_{625} magnitude within each class. Panel pairs are numbered 1 to 59 in the upper right corner of the left-hand panel in each pair. For each pair of panels we also list the type of photometry presented (ALLFRAME or ALLSTAR), and the type of exposures from which the CMDs were derived (“long,” “short” or “short r”). In most cases we present the photometry derived from the long R_{625} and B_{435} exposures (“long”); in $H\alpha$ there are no short exposures in any case. In some cases, however, either the candidate itself or a near neighbor was saturated in the long R_{625} exposures and/or long B_{435} exposures. In cases where saturation affected the reliability of the photometry in long exposures we present

CMDs derived from either the short R_{625} and long B_{435} exposures (“short r”) or short R_{625} and short B_{435} exposures (“short”), depending on whether only the long R_{625} exposures were affected or both the long R_{625} and long B_{435} exposures. Finally, in the upper left corner of the right-hand panel in each pair we list a category for each of the optical counterparts identified—see §3. In some cases these designations are necessarily tentative.

In Table 1 we list all quality 0 and 1 candidate optical counterparts found in these 59 patches. Column 1 lists the X-ray source ID from HCD09. Columns 2, 3, and 4 are the ID number, and x and y coordinates from the ALLFRAME (or ALLSTAR) reductions of the corresponding 401×401 pixel patch.¹³ The radial offsets

¹³ Coordinates correspond to the “r1” patch image if available and otherwise to the “r3” image.

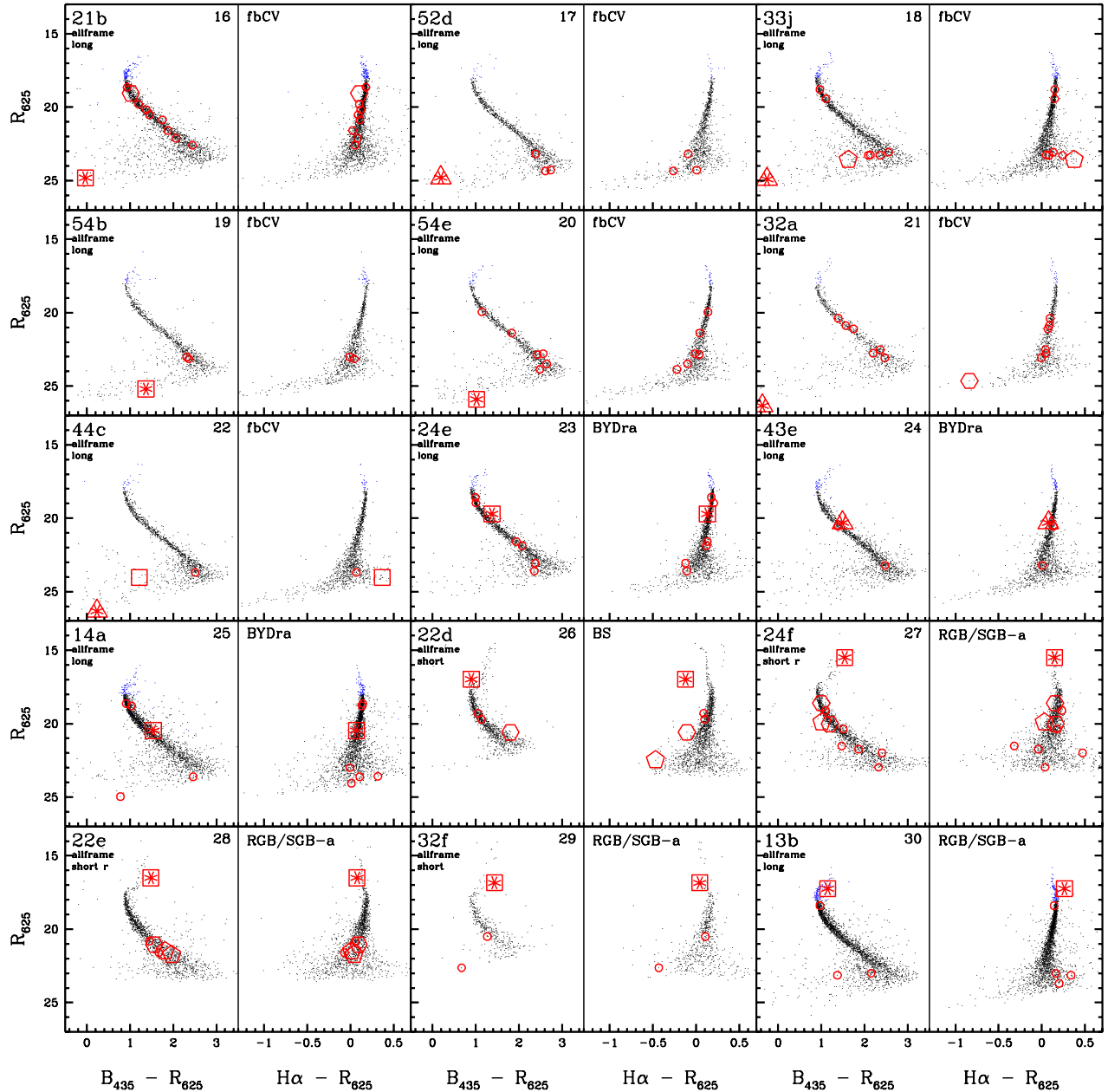


Figure 3. continued

in pixels from the boresight-corrected *Chandra* positions are given in column 5, and the quality of the candidates (0 or 1) appear in column 6. Column 7 gives the classification assigned to each counterpart in this paper.

In 49 of the patches, a single quality 0 or 1 object was found; it is marked with an asterisk in Fig. 3 as the most probable optical counterpart of the X-ray source. In 10 cases, two quality 0 or 1 objects were found in the error circle (see Fig. 3). In these cases, the two potential counterparts are listed together in Table 1, with the most probable ID listed first. In all but 3 cases we choose the object closest to the center of the error circle as the more probable counterpart and mark it with an asterisk. The exceptions are 21d, 22f, and 23b, for which the candidate closest to the center was a blue star which was on the main sequence in $H\alpha - R_{625}$; such stars have a relatively high likelihood of being chance coincidences (see

§3.8). For 23b we consider an object that is both blue and $H\alpha$ -bright (a possible CV) to be the more probable counterpart; for 21d, we consider an $H\alpha$ -bright star the more probable counterpart; and for 22f we consider an extended object to be the more probable counterpart (a likely AGN). These objects are marked with an asterisk in Fig. 3.

We have verified that in excluding quality 2 objects from consideration we are not missing significant numbers of objects that would be promising optical counterparts. Of the 59 sources for which we report identifications, 13 error circles include one or more quality 2 objects. In only four cases (13a, 33m, 41g, and 41h) is a quality 2 object closer to the center of the error circle than the counterpart we report in Table 1. A close inspection of the results in each of these cases confirms that the quality 2 candidates in question are likely to lie off

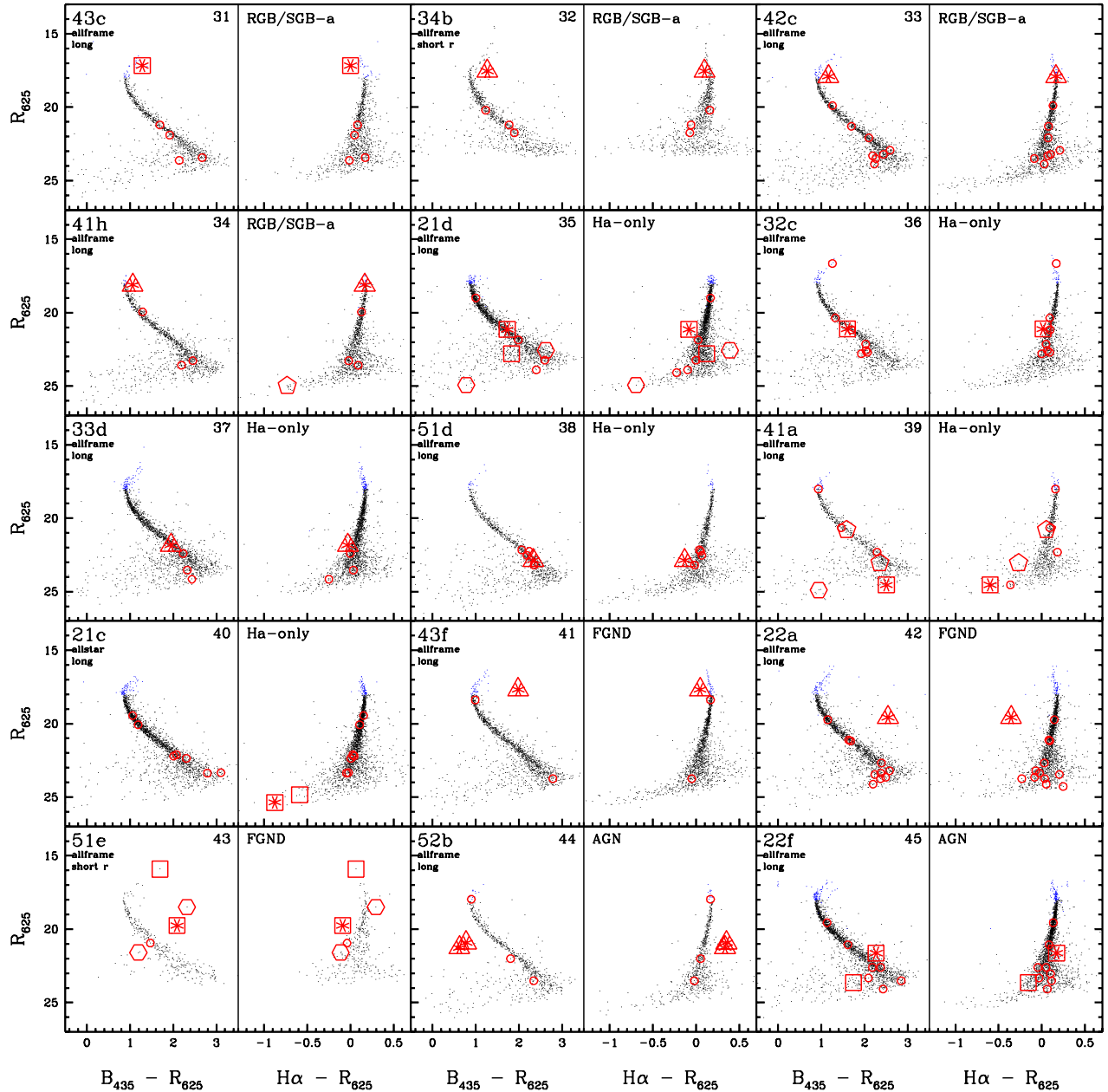


Figure 3. continued

the principal sequences as a result of poor measurements and as such are unlikely to be the true counterparts of the X-ray sources.

J2000 coordinates for all of the candidates appear in columns 8 and 9 of Table 1. Offsets from the cluster center determined by Anderson & van der Marel (2010), R.A. = 13:26:47.24, Dec. = 47:28:46.45 (J2000) appear in column 10. The coordinates provided here are tied to the mosaic image created by Anderson & van der Marel (2010) and can thus be used to locate the stars on the mosaic image provided with that paper. We note that the mosaic was constructed using updated distortion corrections relative to what had been used earlier to locate the centers of the patches for the present work. In most cases the differences are negligible, though they can be as large as $\sim 0''.2$. In a small number of cases this puts the candidate optical counterpart slightly outside a $0''.6$

error circle, but still well within a $1''$ circle.

The small changes in X-ray source positions resulting from the new distortion correction do not alter our choices of which objects are the most likely counterparts in the 10 cases where there are two objects to choose from. In six of those cases, the star that is closest to the center of the $0''.6$ error circle in the patch is also closest to the newly determined position on the mosaic image. In two of the three cases where we had selected an object that was farther from the center of the error circle as the most likely counterpart (22f and 23b), the chosen object turns out to be closer to the new position, lending support to our choice. In only two cases (21c and 51e) does the star that had been closer to the center of the error circle now lie farther away from the newly determined position. In both these cases, the difference in offsets from the new position is small ($\sim 0''.1$), such that posi-

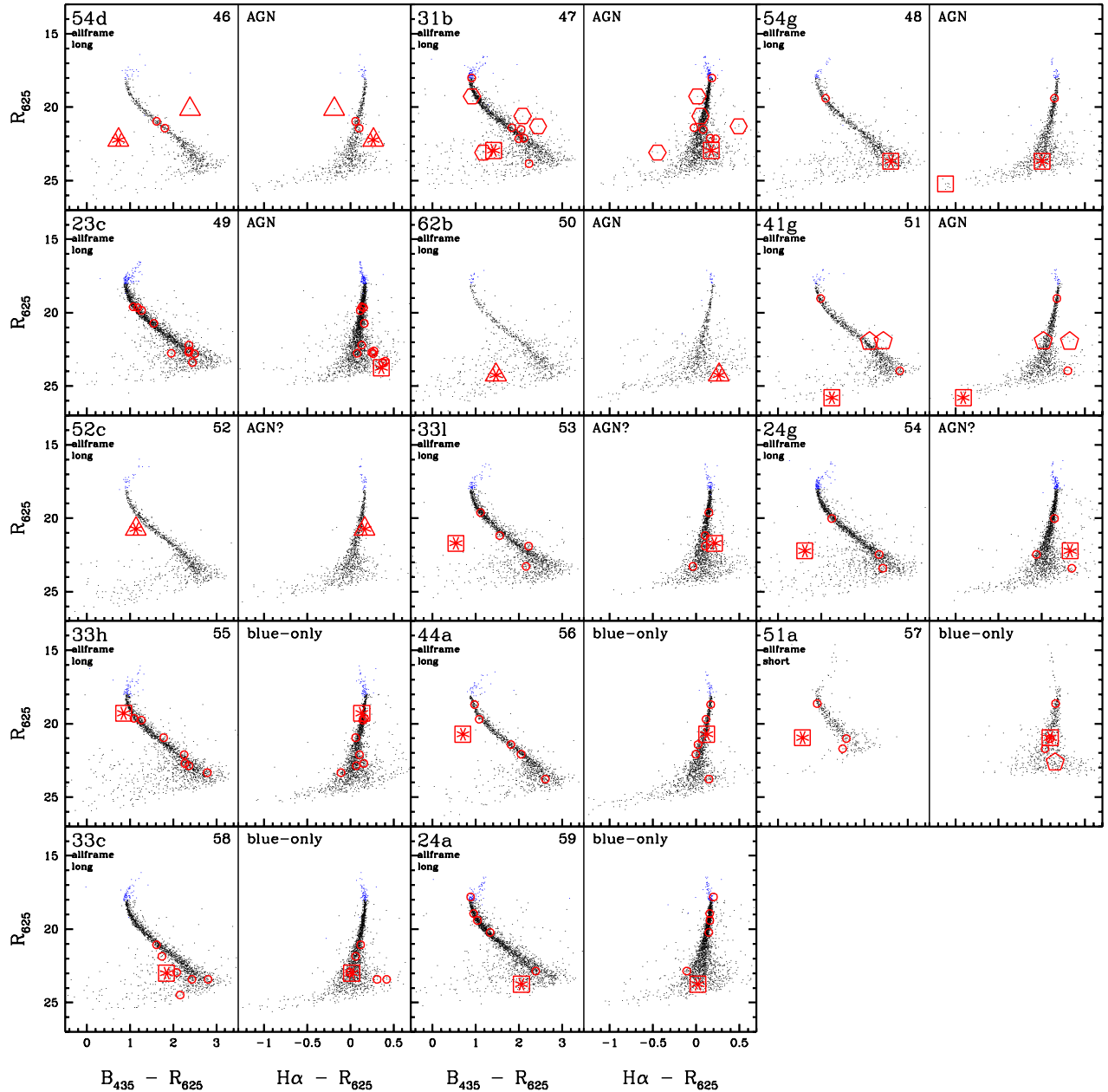


Figure 3. continued

tion alone is not a very useful discriminant. In the case of 51e, where both potential counterparts are probable foreground stars, we consider the original choice to be the best one. This star shows clear emission in $H\alpha$ (see panel 43 in Fig. 3), which is strongly associated with emission in X-rays. In the case of 21c, both potential counterparts are in the “ $H\alpha$ -only” category and lie in a similar location in the $H\alpha - R_{625}$ CMD (see panel 40 in Fig. 3). As there is little to distinguish between the two, we choose not to alter our original selection.

In Table 2 we provide photometric information about each candidate counterpart along with its tentative classification. In the cases for which two potential counterparts were identified, the alternate counterparts are listed separately at the end of the Table. Entries are sorted by classification and then by R_{625} magnitude, to match the sequence in which CMDs appear in Fig. 3. The X-ray

ID, R_{625} magnitude, $B_{435} - R_{625}$ color, and $H\alpha - R_{625}$ color appear in columns 1–4, respectively. Column 5 indicates whether the object appeared blue or red relative to the main sequence (or giant branch). Column 6 indicates whether the object appears “ $H\alpha$ -bright” (to the left of the main sequence) or “ $H\alpha$ -faint” (to the right). Objects that land on the main sequence (or giant branch) are listed as “neither” in these columns. Columns 7 and 8 list the quality and classification of the counterparts, and column 9 lists the X-ray-to-optical flux ratio.¹⁴ For sources likely to be associated with the cluster, column 10 gives the X-ray luminosity for an assumed distance of 4.9 kpc and hydrogen column density of $9 \times 10^{20} \text{ cm}^{-2}$.

As an additional test of the validity of potential coun-

¹⁴ X-ray fluxes from HCD09 have been revised downward by a factor of 1.25 (see §4.1).

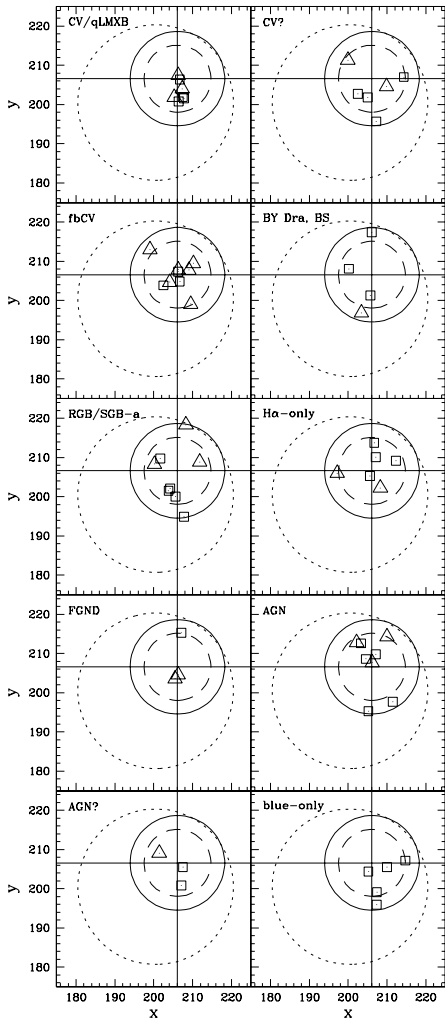


Figure 4. Location within X-ray error circles of optical counterparts listed in Table 1. Dotted line shows initial $1''$ -radius error circle, solid line shows $0.6''$ -radius error circle adopted for detailed search. Dashed line encompasses half of the area of the $0.6''$ error circle (see §2.2 for details). Symbols as in Fig. 2.

terparts we examined where they landed in the X-ray error circles. Fig. 4 shows the location of each of the 59 possible optical counterparts listed in Tables 1 and 2 and shown in Fig. 3, dividing the objects into 10 categories (see column 8 of Table 2). In each of the 10 panels we show the original $1''$ X-ray error circle (dotted line), the final $0.6''$ circle (solid line with cross hair), and a smaller circle of radius $0.424''$ encompassing half of the area of the $0.6''$ error circle (dashed line). We refer to these results in §3 below, as we examine each category of optical counterpart in turn.

3. IDENTIFICATION OF OPTICAL COUNTERPARTS

3.1. Blue, $H\alpha$ -bright stars: cataclysmic variables and a qLMXB

We first consider sources for which we have identified an optical counterpart that is both blue and $H\alpha$ -bright. This combination of signatures is strongly indicative of a compact accreting binary, with the $H\alpha$ excess attributable to an emission line from an accretion disk

and the blue color to the disk and/or the white dwarf. Optical counterparts for 13 of the X-ray sources have this signature. The first of these, shown in panel 1 of Fig. 3, is the qLMXB reported by Haggard et al. (2004). This object was first identified as a qLMXB on the basis of its X-ray spectrum (Rutledge et al. 2002) and is the only X-ray source in ω Cen with both the soft spectrum and the luminosity characteristic of qLMXBs (HCD09).

The next three panels in Fig. 3 show three objects that were first identified in our WFPC2 study of ω Cen (Carson et al. 2000). Panels 2 and 3 show the optical counterparts of ROSAT sources “XA” and “XB,” respectively, both of which Carson et al. identified as probable CVs on the basis of significant $H\alpha$ and UV excesses. Both are clearly $H\alpha$ -bright in the ACS data and 13c (=XA) is also very blue. Interestingly, however, 13a (=XB) is only very slightly blue relative to the main sequence in the new data. This suggests a relatively weak disk in the system and/or significant variability. A third star identified by Carson et al. as a possible counterpart for ROSAT source “XC” (*Chandra* source 12a) is shown in panel 4 (also see Fig. 2). In the 1997 WFPC2 data this star was $H\alpha$ -bright but showed no UV excess (Carson et al. 2000). Here it appears distinctly blue as well as being $H\alpha$ -bright. We conclude that it is likely to be a CV; variability could account for the apparent change in color between 1997 and 2002.

In panels 5 – 7 of Fig. 3 we show, in order of R_{625} magnitude, three new CV candidates that are both blue and $H\alpha$ -bright. They are the counterparts of X-ray sources 54h, 41d, and 24c. The optical counterpart to 54h is easily confirmed visually as being blue, and all the individual $H\alpha - R_{625}$ measurements (from single $H\alpha$ and R_{625} frames) consistently show it is $H\alpha$ -bright. The counterpart to 41d is easily visually confirmed as being $H\alpha$ -bright, and the individual $B_{435} - R_{625}$ measurements consistently show it is blue. The counterpart to 24c is visually confirmed as being both blue and $H\alpha$ -bright. These three stars are listed along with the optical counterparts of X-ray sources 13c, 13a, and 12a as “CVs” in Tables 1 and 2.

Six additional CV candidates are shown in panels 8 – 13, in order of increasing magnitude, from $R_{625} = 22.0 - 25.2$. Each of these stars is visually confirmed as being either blue or $H\alpha$ -bright. Somewhat lower confidence in either their blue color or $H\alpha$ excess (see Table 2, columns 5 and 6) leads us to give them the more tentative designation “CV?” in Tables 1 and 2.

The top left panel of Fig. 4 shows the positions within their respective error circles of the six most secure CV counterparts along with the qLMXB (44e). These stars are tightly clustered near the center of the error circles and well inside even the inner dashed circle, leaving little doubt that they are the counterparts of the X-ray sources. The top right panel shows the six tentative CV counterparts. While not as tightly clustered in the centers of the error circles, five of the six land inside the inner, dashed circle (whose area was chosen to be one half that of the $0.6''$ circle), the probability of which is $6 \times (0.5)^6 = 9.4\%$ if the stars were unrelated to the X-ray sources. Larger positional uncertainties are also to be expected for a population of objects that are fainter on average in both X-ray and optical light. This fur-

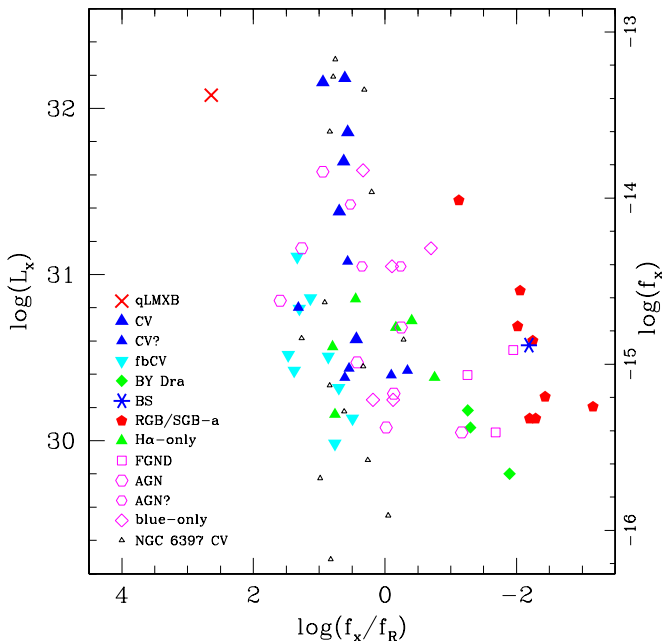


Figure 5. X-ray luminosity in erg s^{-1} and flux in $\text{erg s}^{-1} \text{cm}^{-2}$ vs. X-ray-to-optical flux ratio for optical counterparts identified using *HST* data. X-ray fluxes and luminosities are in a 0.5 – 2.5 keV band, adopted from HCD09, but revised downward by a factor of 1.25 (see §4.1). Large solid symbols represent candidates likely to be members of ω Cen while large open symbols represent non-members (and probable non-members). For comparison, small black open triangles are CV candidates identified by Cohn et al. (2010) in NGC 6397; only the L_x scale applies for these points.

ther supports our conclusion that these are the probable counterparts of the X-ray sources.

Further insight into the nature of the potential optical counterparts can be gained from their X-ray-to-optical flux ratios and their luminosities. In Fig. 5 we plot the X-ray luminosity of each object against the ratio of its X-ray to R_{625} -band flux. X-ray fluxes are in the 0.5 – 2.5 keV band and assume a 1 keV thermal bremsstrahlung spectrum (HCD09); luminosities were computed assuming a distance to the cluster of 4.9 kpc. Large blue triangles denote the six CV candidates with clear-cut blue colors and $H\alpha$ emission. Smaller blue triangles denote the tentative CV candidates. Four of these have flux ratios very similar to those of the other CVs. The other two have somewhat lower flux ratios, but still resemble the CVs in this diagram more than other types of systems (e.g. active binaries, which have much lower X-ray-to-optical flux ratios; see below). We conclude that these six optical counterparts are also likely to be CVs.

3.2. Faint blue stars: more cataclysmic variables?

Very faint blue stars were found in the error circles of nine of the *Chandra* sources. They have magnitudes in the range $R_{625} = 24.5 - 26.3$ and are shown in Fig. 3, panels 14 – 22. All but one (54e) are confirmed visually as being blue by blinking R_{625} vs. B_{435} images. None of these stars are detected in $H\alpha$ with ALLFRAME—thus they do not appear in the $H\alpha - R_{625}$ diagrams. These stars lie in the region of the CMDs generally occupied by white dwarfs; in the absence of X-ray emission one

might simply assume that is what they are. Thus we need to consider whether this many white dwarfs could have landed by chance in the *Chandra* error circles. The $109 \text{ } 0''.6$ radius error circles occupy about 0.03% of the $10' \times 10'$ field. Monelli et al. (2005) used these data to study the WD sequence and found 2212 WDs in 1/3 of the total area covered. One would therefore expect $\sim 3 \times 2212 \times 0.0003 \simeq 2$ WDs to fall within the *Chandra* error circles by chance. Considering that all but one land in the inner half of the error circle (see Fig. 4, “fbCV” panel), this number reduces to ~ 1 . The probability that this would happen if the stars were unassociated with the X-ray sources is 1.8%. We conclude that these stars are the likely sources of the X-rays and not simply WDs that have landed by chance in the X-ray error circles.¹⁵

These nine stars are exceedingly faint, with absolute magnitudes in the range $M_{625} \simeq 10.7 - 12.5$ at the distance of ω Cen. Most are seen in B_{435} only because they are so blue; main sequence stars of comparable R_{625} magnitude are below the detection limit. In view of this, the lack of $H\alpha$ detection does not necessarily imply that they are not $H\alpha$ -bright; they may simply be too faint to be detected, even in the presence of an $H\alpha$ emission line. Indeed, only one of the moderately bright CV candidates (44d), is fainter than even the brightest of these nine stars, and its $H\alpha$ status is uncertain. The faintest CV candidate for which excess $H\alpha$ emission is clear cut (24c) is 1 magnitude brighter than the brightest of these stars and 2–3 magnitudes brighter than most of them. As discussed in §4 below, we suggest that these stars are likely to be very faint cataclysmic variables near the period limit, similar to those identified in the Sloan Digital Sky Survey (SDSS; Gänsicke et al. 2009) and in NGC 6397 (Cohn et al. 2010). Their positions in the X-ray luminosity vs. f_X/f_R diagram (inverted light blue triangles in Fig. 5) are also consistent with this interpretation. The median value of the ratio of soft to hard X-ray counts reported by Haggard et al. (2009) for these sources (see their Table 1) is 1.2. This is consistent with their being CVs (cf. Fig. 6 of Haggard et al. 2009), and argues against the possibility that they could instead be MSPs with low-mass white dwarf companions (which can appear in a similar part of an optical CMD—see Edmonds et al. 2001); MSPs typically have much softer X-ray colors (see, e.g., Fig. 9 of Heinke et al. 2005). We refer to these stars hereafter as “faint blue CVs” (fbCVs).

3.3. BY Draconis stars and a possible blue straggler

Narrow-band $H\alpha$ imaging also enables us to search for binaries in the form of BY Draconis stars. These systems show $H\alpha$ in emission due to elevated levels of coronal activity resulting from rapid spin rates typically as a result of tidal synchronization with a companion star (Dempsey et al. 1997 and references therein). Such stars have been found in a number of globular clusters to date (e.g., Taylor et al. 2001, Albrow et al. 2001, Pooley et al. 2002, Huang et al. 2010, Cohn et al. 2010).

¹⁵ The fact that these stars lie within the inner half of their respective error circles also confirms that the adopted error circle radius of $0''.6$ is sufficiently generous even for faint X-ray sources. The new distortion correction confirms this conclusion, with 8 of the 9 lying less than $0''.35$ arcseconds from the newly determined mosaic positions.

Considering the typical emission line strengths of such systems ($\text{EW}(\text{H}\alpha) \lesssim 5$ Angstrom, e.g. Chevalier & Ilovaisky 1997), and the ~ 80 Angstrom width of the ACS/WFC $\text{H}\alpha$ filter, such stars will have $\text{H}\alpha$ excesses (relative to normal main-sequence stars) $\lesssim 0.06$ magnitudes in the present study. This is sufficiently small that we expect only to be able to detect the subset with the strongest lines. To limit the number of false positives, we required that a star show both an $\text{H}\alpha$ signature and also lie redward of the main-sequence ridge line in the $B_{435} - R_{625}$ CMD. The latter requirement excludes binaries whose mass ratios are much less than unity. The three possible BY Dra stars found in this way are shown in Fig. 3, panels 23 – 25, and are designated “BYDra” in Table 2. The f_X/f_R ratios for these stars are much lower than for accretion-driven systems, on the order of 10^{-2} (see green diamonds in Fig. 5), consistent with their tentative identification as stars with active coronae. Their X-ray luminosities ($\sim 10^{30}$ erg s^{-1}) are also consistent with their being coronal sources (cf. Dempsey et al. 1997).

A further test of the viability of these three counterparts can be made by examining the ratio of their X-ray to bolometric luminosities, a quantity that has been shown to depend on stellar rotation and to saturate at a maximum value of $\log(L_x/L_{\text{bol}}) \sim -3$ (Stauffer et al. 1994, Güdel 2004, and references therein). Using bolometric luminosities derived from the stellar models of Bedin et al. (2005) appropriate for the dominant metallicity group in ω Cen, together with the L_x values given in Table 2, we find that the proposed optical counterparts for 24e, 43e, and 14a would have $\log(L_x/L_{\text{bol}}) = -3.1, -2.5,$ and -2.4 , respectively. That two of the three have ratios that are a factor of ~ 3 higher than the known limit suggests that at least some of these stars may not be the counterparts of the X-ray sources.¹⁶ Given the many uncertainties that go into computing these ratios (e.g., the X-ray sources in question are very faint), we report the counterparts nonetheless, as they remain the best prospects we have found for BY Dra stars in ω Cen.

Another candidate optical counterpart (22d; see panel 26) appears above the turnoff, to the blue side of the subgiant branch. A close-up of this region is shown in Fig. 6, based on photometry of 1.2 million stars in the cluster from Anderson & van der Marel (2010); for clarity, only half the stars are shown in this plot. The star lies directly above the turnoff associated with the dominant population of stars in the cluster. Its f_X/f_R flux ratio and X-ray luminosity (see blue asterisk in Fig. 5), and $\log(L_x/L_{\text{bol}}) = -3.5$, are all within observed values for coronal sources. This suggests that it could be a rapidly-rotating blue straggler, a blue straggler with an active main-sequence star companion (see, e.g., Knigge et al. 2006), or perhaps a BY-Dra-type system that contains two turnoff stars. Notably, however, the star has a rather large $\text{H}\alpha$ excess (0.25 mag; see Fig. 3 panel 26), corresponding to an emission line strength of $\text{EW}(\text{H}\alpha) \sim 20$ Angstroms. This is unusually strong for coronal sources, for which $\text{EW}(\text{H}\alpha)$ is typically an order of magnitude

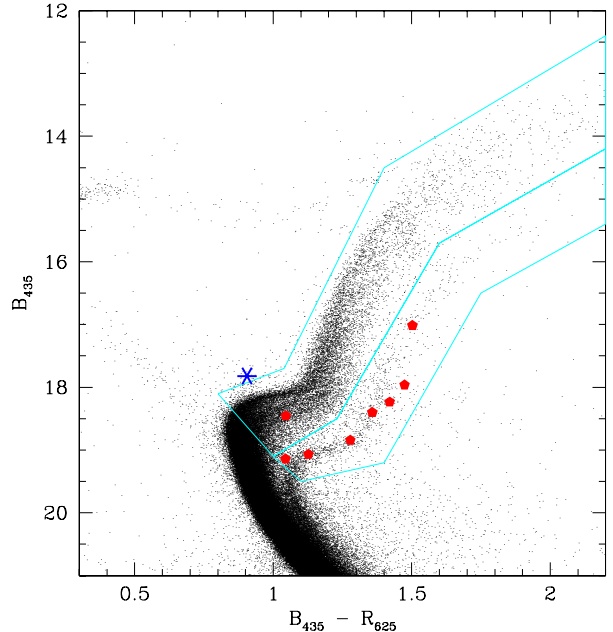


Figure 6. Close-up of the turnoff, subgiant, and giant regions of ω Cen, from the photometry of Anderson & van der Marel (2010). To best delineate the different RGB and SGB sequences, we plot only about half of the stars. Seven of the optical counterparts we have identified lie on or near the anomalous RGB or SGB, which is significantly redder than the other RGB and SGB sequences in the cluster. For simplicity, we include an eighth star (counterpart of 13b) in the classification although it lies along one of the other subgiant sequences. The blue asterisk marks a star identified as a possible turnoff binary or blue straggler (see §3.3). Regions outlined in cyan are used to determine the significance of having found 7 X-ray-bright stars apparently associated with the RGB/SGB-a sequence (see §3.4).

or more lower (cf. Young et al. 1989). Alternatively, it could be a CV in which the white dwarf is accreting from a subgiant. In this case the high optical luminosity of the subgiant might account for the rather low f_X/f_R ratio.

3.4. Stars on or near the anomalous subgiant and giant branch

Eight of the candidates we have identified lie redward of and/or below the giant and subgiant branches formed by the dominant population in the cluster (the most metal-poor population, with $[\text{Fe}/\text{H}] = -1.7$; “group A” in the nomenclature of Villanova et al. 2007). They have magnitudes in the range $R_{625} = 15.5 - 18.1$ and colors in the range $B_{435} - R_{625} = 1.1 - 1.5$ (see Fig. 3, panels 27 – 34). To assess the possible connection between these stars and the complex of giant and subgiant branches in ω Cen, in Figure 6 we plot a CMD for the full ACS/WFC field from the photometry of Anderson & van der Marel (2010). Here the multiple giant and subgiant branches are well populated and readily identified. The eight stars of interest all appear in the catalog created by Anderson & van der Marel (2010) and are marked with red pentagons. Seven lie on or very close to the so-called anomalous red giant and subgiant branches in the cluster (RGB-a and SGB-a; Pancino et al. 2000, Ferraro et al. 2004). Given their locations in the CMD, we designate these stars “RGB/SGB-a” in Table 2. However, as discussed below (see §4.2), in the absence of metal-

¹⁶ Correcting for the differing bandpasses in which L_x values are reported by, e.g., Stauffer et al. (1994) vs. Haggard et al. (2009) increases the ratios we obtain by an additional factor of ~ 1.5 , making the discrepancy worse.

licity measurements, it is unknown whether these stars are actual members of this metal-rich “anomalous” population in ω Cen, or if they lie in this part of the CMD for other reasons. For simplicity we also include in the “RGB/SGB-a” category the eighth star, a possible counterpart of 13b (Fig. 3, panel 30), though it is clearly not a member of the anomalous population. It lies along the subgiant branch associated with the “group C” population identified by Villanova et al. 2007, and is ~ 0.3 - 0.4 magnitudes fainter in B_{435} than the (“group A”) giant and subgiant branches (Fig. 6).

Before addressing the potential significance of these stars, we must determine whether their apparent association with X-ray sources could be the result of chance coincidence. Adopting the lower outlined region shown in Fig. 6 that roughly encompasses the SGB-a and RGB-a stars, we find that there are a total of ~ 3000 such stars in the ACS/WFC field of view. Given that all of the $0''.6$ error circles combined cover only $\sim 1/3000$ of the total area of the mosaic, we would expect ~ 1 of these stars to have landed by chance in the X-ray error circles. That 7 of them appear in X-ray error circles strongly supports the view that they are the sources of the X-rays (chance probability $\simeq 2 \times 10^{-5}$).

Two additional arguments favor these stars being the sources of the X-ray emission. First, three show signs of $H\alpha$ in emission, which is strongly associated with enhanced X-ray emission. Second, the X-ray luminosities and f_X/f_R ratios for these stars are typical of stars with active coronae (see red pentagons in Fig. 5).

Having demonstrated that they are the likely sources of the observed X-ray emission, we must also ask whether these stars are associated with the cluster. Proper motions can be used to determine membership, but require measurements in two well-separated epochs of imaging, which is beyond the scope of the present paper.¹⁷ In the absence of proper motions, we consider instead what other explanation there could be for a group of stars in this region of the CMD. As they are redder than typical stars in ω Cen, one possibility is that they could be foreground stars. However, it is highly improbable that such a large number of foreground stars would be confined to a small region of color-magnitude space. At fainter magnitudes, where foreground stars would be expected to be more prevalent given the larger volume encompassed, we find only two foreground stars (see §3.6). The stars in question also have $B_{435} - R_{625}$ and $H\alpha - R_{625}$ colors quite different than those of the faint foreground stars (see §3.6). We conclude that the stars that we have identified in the vicinity of the RGB/SGB-a are likely to be associated with ω Cen.

It is also of interest to determine whether the frequency of X-ray bright stars among RGB/SGB-a stars is larger than among other giants and subgiants in the cluster. To this end, we counted the number of stars in the upper outlined region shown in Fig. 6, that encompasses groups A, B and C as defined by Villanova et al. 2007 (i.e., all giants and subgiants that are not part of the anomalous branches). A total of $\sim 30,000$ stars lie in this portion of the CMD. Of these, we would expect about 1 in 3000, or

~ 10 , to have landed in the X-ray error circles by chance. Searching through the CMDs we constructed for all the X-ray source error circles, we find 14 “normal” giants in total, consistent with them all being chance alignments. Thus, despite the fact that there are ~ 10 times more stars on the upper subgiant and giant branches, only twice as many land in X-ray error circles than do the SGB-a and RGB-a stars. This implies that X-ray sources are at least 5 times overabundant among the SGB-a and RGB-a stars relative to the normal giant and subgiant branch stars. Taking account of the fact that only ~ 4 of the normal RGB/SGB stars found in error circles are likely to be true X-ray source counterparts (vs. ~ 6 of the anomalous RGB/SGB stars), the implied overabundance rises to a factor of ~ 15 . The significance of these stars and their possible association with stars found in similar regions of the CMD in other clusters (e.g., so-called “red stragglers” and “sub-subgiants”) will be discussed below (see §4.2).

3.5. Stars with $H\alpha$ excess only: CVs or BY Dra binaries?

Six stars were identified that show signs of $H\alpha$ in emission but land on the main sequence in the $B_{435} - R_{625}$ CMD—or, in one case, are not detected in the blue filter (see panels 35-40 in Fig. 3). While the emission is quite weak in some cases, the fact that five of these six possible counterparts lie in the inner half of the error circles (see Fig. 4) suggests that most are likely to be genuine counterparts of the X-ray sources. In Tables 1 and 2 we designate these stars as “ $H\alpha$ -only.”

Objects with this $H\alpha$ signature could be CVs with weak disks, such as have been seen in NGC 6397 (Cool et al. 1998, Cohn et al. 2010). In ω Cen itself, the optical counterpart of source 13a, which was previously determined to be a CV (Carson et al. 2000), is only very slightly blue in the present data, and the counterpart of 12a, seen to be quite blue here, was formerly seen to be on the main sequence (Carson et al. 2000). Some of these stars could alternatively be BY Dra-type main-sequence binaries, in which the secondary star is too faint to noticeably alter the color of the combined system.

A potentially distinguishing feature between X-ray sources powered by accretion and those resulting from active coronae is the ratio of X-ray-to-optical flux. In Fig. 5 we see that three of the $H\alpha$ -only stars (green triangles) lie solidly in the region occupied by CVs. Two others are near the edge of the CV region, while the third lies between the CV region and the region occupied by coronal sources. We conclude that the perhaps 4 or 5 of these sources are likely to be CVs, while one or more could instead be BY Dra-type binaries.

3.6. Foreground stars

Three of the optical counterparts have magnitudes and colors that place them $\gtrsim 1$ magnitude redward of the cluster main sequence or turnoff (see Fig. 3, panels 41-43). Their $B_{435} - R_{625}$ colors are in the range 2.1 – 2.5, suggestive of late K or early M stars. All three also have significant $H\alpha$ excesses (~ 0.15 - 0.5 magnitudes) and X-ray-to-optical flux ratios that are typical of coronal sources (see magenta squares in Fig. 5). We conclude that these are most likely foreground dwarfs with active

¹⁷ The only one of these stars (13b) that appears in the proper-motion catalog of Anderson & van der Marel (2010) has motions consistent with membership.

coronae (e.g., dMe or dKe stars), which are very common in the field (Riaz, Gizis, & Harvin 2006). Two such stars have already been identified in the foreground of ω Cen (Cool et al. 1995a). We note that the brightest of the three (43f) has an R_{625} magnitude of 17.7, in the same range as the RGB/SGB-a stars discussed in §3.4. However, its very red $B_{435} - R_{625}$ color and prominent $H\alpha$ emission make it appear more like the two other fainter foreground stars and we therefore include it in this class.

3.7. Active galactic nuclei

Eight of the X-ray source error circles contained visibly extended objects. Given the large number of AGN we expect in the background of this ω Cen mosaic (HCD09), it seems likely that most or all of these are the optical counterparts of the X-ray sources. In most cases no other compelling optical counterpart was found in the error circle. We note that AGN can be useful in determining the absolute motions of globular clusters.

The locations of the AGN within the CMDs are shown in Fig. 3, panels 44–51; magnitudes and colors are necessarily approximate given that we derived them from fitting the PSF to an extended source. Half of the extended sources have a distinctive blue, $H\alpha$ -faint signature (52b, 54d, 31b, 62b); one of these (52b) was double-peaked in the image and appears as two triangles in the CMDs. Seven of the eight have relatively high X-ray-to-optical flux ratios (see large magenta hexagons in Fig. 5), consistent with their identification as accretion-powered X-ray sources.

Three additional objects were found in the X-ray error circles that appeared to be point-like, but had the same blue, $H\alpha$ -faint signature found for half of the extended sources. These objects are shown in panels 52-54 of Fig. 3. Given that this combination of blue color and $H\alpha$ deficit was uniquely associated with several clearly extended objects, we tentatively identify these objects as AGN, and designate them “AGN?” in Tables 1 and 2. Their X-ray-to-optical flux ratios are also consistent with this designation (see small magenta hexagons in Fig. 5). It is likely that the crowding and high background levels in the images could mask any extended emission that might be present.

3.8. Other blue stars

Blue stars with $R_{625} = 19.3 - 23.8$ were found in the error circles of five *Chandra* sources (see Fig. 3, panels 55–59). In contrast to the very faint blue stars discussed above, these stars are bright enough to be readily detected in $H\alpha$. All fall on the main sequence in $H\alpha - R_{625}$ and thus show no sign of $H\alpha$ in emission. In Tables 1 and 2 we designate these stars as “blue-only.”

The two faintest of these (33c and 24a) are in a region of the diagram that is populated by numerous background stars. The most probable explanation for these is that they are background stars that have landed by chance in the X-ray error circles.

The three brighter stars (33h, 44a, and 51a), by contrast, are in a region of the CMD that is quite sparsely populated, and are thus much less likely to be chance alignments. Two have $B_{435} - R_{625}$ colors significantly bluer than the turnoff, making it improbable that they are background stars. One possibility is that they are

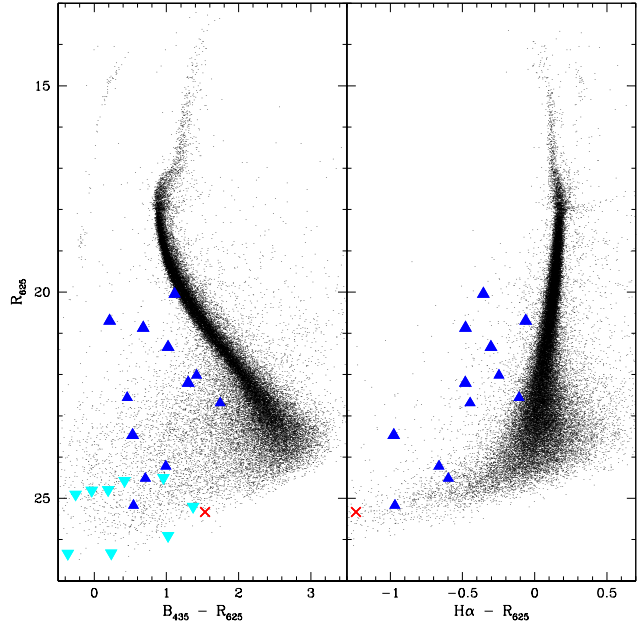


Figure 7. Color–magnitude diagrams showing 12 CV candidates that are both blue and $H\alpha$ -bright, together with 9 that are very faint and blue but undetected in $H\alpha$. The qLMXB is also shown. Symbols as in Fig. 5. Six more tentative “ $H\alpha$ -only” CV candidates, some of which could be BY Dra stars (see §3.5), are not shown.

CVs with weak emission lines. At the magnitudes of these stars, $EW(H\alpha)$ would need to be $\gtrsim 5$ -10 Angstroms to produce a detectable $H\alpha$ excess. Emission lines this weak are not unknown among CVs. Alternatively, one or more of these objects could be AGN. Either interpretation would be consistent with their f_X/f_R values, which are similar to those of CVs or AGN (see open magenta diamonds in Fig. 5).

4. DISCUSSION

The ACS/WFC mosaic encompasses 109 of the 180 known X-ray sources in and toward ω Cen. Using B_{435} , R_{625} , and $H\alpha$ imaging we have identified promising optical counterparts for more than half of these sources. The optical counterparts divide into several categories. Probable cluster members include cataclysmic variables, a quiescent low-mass X-ray binary, possible BY Draconis stars, and a possible blue straggler. They also include a new class of sources that appear to be associated with the cluster’s anomalous RGB and SGB populations. Finally, we identify three probable foreground stars and at least eight AGN behind the cluster.

4.1. The CV population in ω Cen

The single largest class of optically identified X-ray sources in ω Cen is cataclysmic variables (see Fig. 7). We find 27 candidates, only three of which were previously known (Carson et al. 2000). This is among the largest number of CV candidates yet identified in a globular cluster, comparable to the population found in 47 Tuc (Edmonds et al. 2003a,b; Heinke et al. 2005). The candidates span more than 6 magnitudes in apparent brightness, with $R_{625} = 20.0 - 26.3$. Adopting a distance modulus of $(m-M)_{625} = 13.8$ (Haggard et al. 2004), this corresponds

to absolute magnitudes in the range $M_{625} = 6.3 - 12.6$. There is a hint of bimodality in the distribution (blue and cyan symbols in Fig. 5), possibly indicative of a period gap, with just one CV in the range $R_{625} = 23 - 24$ ($M_{625} \simeq 9.2 - 10.2$), and more than half of the candidates being fainter than $R_{625} = 24$.

The absolute magnitudes of the faint CV candidates are similar to those of the faintest CVs discovered in the SDSS (Szkody et al. 2011), which have been shown to have orbital periods of 80 – 86 min, at or near the theoretical limit for CVs (Gänsicke et al. 2009). That discovery resolved a long-standing controversy concerning the theory of late-stage evolution of CVs, which predicts a pile up of old, faint systems near the period minimum. The subset of these faint, short-period SDSS CVs for which distances have been determined have absolute magnitudes in the range $M_g = 10.5 - 13.1$; given their $g - r$ colors (Gänsicke et al. 2009), their V -band magnitudes should be similar. This is to be compared to $M_{625} = 10.4 - 12.6$ for the ω Cen CVs, for which we expect colors in the range $V - R \sim 0.0 - 0.5$, given their observed $B_{435} - R_{625}$ colors. The similarity in absolute magnitudes of these systems suggests that we have identified a population of short-period, low-accretion-rate CVs in ω Cen.

ω Cen is the second globular cluster in which such a faint population of CVs has been found. A similar group was identified in NGC 6397 by Cohn et al. (2010), with median $M_{625} = 11.2$. Notably, the faint CVs in NGC 6397 lie on or close to the WD sequence in a $B_{435} - R_{625}$ vs. R_{625} CMD (see Fig. 3 of Cohn et al.), suggesting that the optical light is dominated by the white dwarf. This is similar to what we observe in ω Cen, though in ω Cen the color spread is larger, due at least in part to measurement uncertainties, as these stars are close to the magnitude limit of the data. In contrast to isolated WDs, the luminosity of the WD in a CV is not a measure of its age, but is instead a measure of the time-averaged accretion rate onto the WD (Townesley & Bildsten 2002). If we assume that the optical flux of the faint CV candidates in ω Cen is dominated by the WDs, the corresponding accretion rates predicted by Townesley & Bildsten (2002) are $10^{-11} - 10^{-9} M_{\odot}/\text{yr}$. Such accretion rates are consistent with periods below the period gap (Patterson 1984; Townesley & Gänsicke 2009; Knigge, Baraffe, & Patterson 2011).

The lack of observed $H\alpha$ emission among many of the faintest CVs in ω Cen (the 9 “faint blue CVs”—see Tables 1 and 2) can also be understood if their spectra are similar to those of the faint CVs in the SDSS. A key spectral signature of SDSS CVs near the period minimum is the presence of broad hydrogen absorption lines superposed on the emission lines that are prototypical of CVs (Gänsicke et al. 2009). This dominance of the WD in the spectrum not only makes the systems very blue (i.e., they lie on or near the WD sequence in a $B_{435} - R_{625}$ vs. R_{625} CMD), but also reduces the excess $H\alpha$ flux relative to the continuum. This alters the $H\alpha - R_{625}$ colors measured from the imaging data in such a way that they appear to have little or no $H\alpha$ excess. In NGC 6397, the effect is particularly noticeable for the five CV candidates that lie on or slightly blueward of the WD sequence. Those five candidates show no $H\alpha$ excess relative to the main sequence. However, they are still clearly $H\alpha$ -bright

by comparison to the WD sequence, which appears as a group of faint stars to the $H\alpha$ -faint side of the main sequence in the $H\alpha - R_{625}$ vs. R_{625} diagram (also see Strickler et al. [2009] for a discussion). Given the relative shallowness of the ω Cen $H\alpha$ data as compared to those obtained for NGC 6397, the lack of observed $H\alpha$ emission among the “fbCVs” appears to be compatible with their being similar to the faint CVs in NGC 6397.

Further insight into the nature of the CVs in ω Cen can be gained by examining their X-ray-to-optical flux ratios. This distance-independent quantity can be directly compared to values for CVs in other clusters and in the field. It is of particular interest to compare these ratios to those for CVs in NGC 6397, since both are X-ray selected samples collected using the same methods. To compute flux ratios for the CVs in ω Cen, we adopt the unabsorbed f_X values reported by HCD09, revised downward¹⁸ by a factor of 1.25, and $f_R = 10^{0.4R-5.89}$. The latter makes use of the average flux per unit wavelength of Vega in the F625W band,¹⁹ the *PHOTBW* width of the filter,²⁰ and includes a correction for an estimated 0.29 magnitudes of extinction toward ω Cen (Haggard et al. 2004). The resulting flux ratios for the CVs in ω Cen are in the range $f_X/f_R \simeq 0.2 - 30$, with a median value $f_X/f_R = 4.2$ (see Fig. 5).

To make a comparison to NGC 6397, we need to account for the different assumptions used to derive X-ray and optical fluxes for CVs in the two clusters. This requires multiplying the X-ray fluxes reported by Bogdanov et al. (2010)²¹ by a factor of 1.17 and dividing optical fluxes reported by Cohn et al. (2010)²² by a factor of 1.18. The resulting X-ray-to-optical flux ratios for the 15 CV candidates in NGC 6397 are in the range $f_X/f_R \simeq 0.5 - 20$, with a median value $f_X/f_R = 5.7$. For ease of comparison to the CV candidates in ω Cen, we have plotted the NGC 6397 CV candidates in Fig. 5 (small open black triangles), assuming a distance of 2.4 kpc. The two sets of candidates occupy a similar part of the L_x vs. f_X/f_R plane, with a similar range of flux ratios and a similar maximum X-ray luminosity. The only apparent difference is the presence of fainter CVs in the NGC 6397. Whether ω Cen also harbors CVs this faint is not yet known, as they are below the detection limit of the *Chandra* imaging reported by HCD09.

As a quantitative test of the similarity or difference between the CV populations in ω Cen and NGC 6397, we use the KS test to compare cumulative distributions of f_X/f_R ratios (see Fig. 8). For NGC 6397, we plot

¹⁸ Here we use <http://asc.harvard.edu/toolkit/pimms.jsp> to convert count rate to flux; fluxes reported by HCD09 used WEBPIMMS, and did not account for the higher sensitivity of the instrument in early years of operation (ω Cen X-ray data were acquired in 2000).

¹⁹ <http://www.stsci.edu/hst/acs/analysis/zeropoints>

²⁰ <http://www.stsci.edu/hst/acs/analysis/bandwidths>

²¹ Beginning with the 0.5 – 6.0 keV counts reported by Bogdanov et al. (2010) (in an effective exposure time of 237 ksec—S. Bogdanov, private communication), and assuming the same spectrum and band as for the ω Cen CVs, we find that 1 count/sec is equivalent to an unabsorbed flux of $5.81 \times 10^{-12} \text{ erg s}^{-1} \text{ cm}^{-2}$ if we use the same N_H adopted by Bogdanov et al. This is a factor of 1.17 higher than the conversion adopted in that paper for a different set of assumptions.

²² Optical fluxes reported by Cohn et al. (2010) assume $f_R = 10^{0.4R-6}$, which results in values 1.18 higher than the conversion adopted in the present paper.

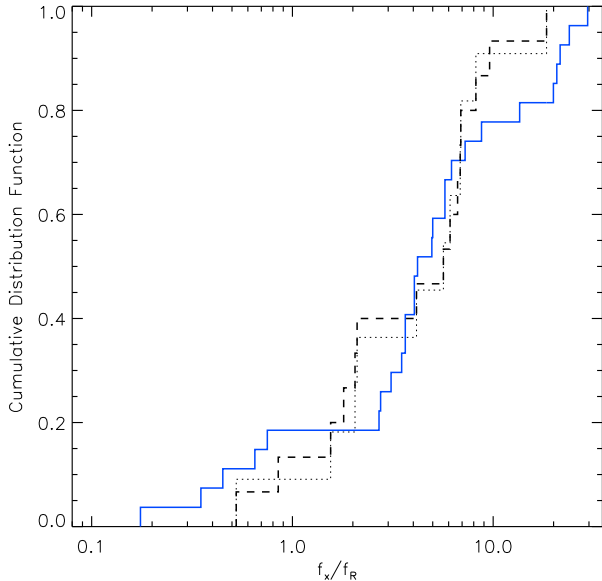


Figure 8. Cumulative distribution of X-ray-to-optical flux ratio for CVs in ω Cen vs. NGC 6397. Solid blue line: CV candidates in ω Cen; dashed black line: CV candidates in NGC 6397 that are bright enough to have been detected in ω Cen; dotted black line: all CV candidates in NGC 6397.

distributions both for the entire population of 15 candidate CVs and for the subset of 11 candidates that are bright enough in both X-rays and optical to have been detected, at least in principle, if they had been in ω Cen. The KS test shows that distributions of f_X/f_R ratios are consistent with having been drawn from the same parent population (KS probability 0.94 when comparing ω Cen CV candidates to the 11 brightest candidates in NGC 6397, and 0.71 when comparing to all NGC 6397 candidates). The Anderson-Darling test, which is more sensitive to deviations near the beginning or end of the distributions, also reveals no significant differences: the P-value is 0.53 when comparing ω Cen CV candidates to those CVs in NGC 6397 that could have been detected in ω Cen, and 0.45 when comparing to the full set of NGC 6397 CVs. To the extent that different f_X/f_R ratios characterize the different subclasses of CVs (see, e.g., Verbunt et al. 1997, Heinke et al. 2008, Agüeros et al. 2009), we find no evidence that the CVs in the two clusters have a different class make-up. Thus, to the extent that it can be discerned from a small number of f_X/f_R ratios, the different formation histories of the CVs in the two clusters (see below) do not seem to have a significant effect on the types of CVs that are created.

We have also compared the flux ratios for CVs in ω Cen to those reported by Edmonds et al. (2003b) for the CVs in 47 Tuc. The median f_X/f_{opt} ratio they report for 17 CVs in that cluster is 1.2—a factor of 3.5 times lower than the median value for CV candidates in ω Cen, and 4.8 times lower than the median for those in NGC 6397. These apparent differences are not due to the different definition of optical fluxes adopted here vs. by Edmonds et al. By directly comparing our f_X/f_R ratios to the f_X/f_{opt} ratios reported for 47 Tuc, we are effectively assuming that the CVs in ω Cen and NGC 6397 have $V - R = 1.15$. If the CVs are bluer (as is likely given their $B_{435} - R_{625}$ colors), then the differences in me-

dian flux ratios would only increase. It is unclear, however, what the significance of these apparent differences is. The faintest counterparts in the 47 Tuc CV sample, which is based on WFPC2 imaging, have absolute magnitudes of $M_V \sim 10$ (Edmonds et al. 2003a). This is to be compared to limits of $M_{625} = 12.6$ and 13.9 in ω Cen and NGC 6397 CV samples, respectively, both of which made use of the higher-resolution ACS/WFC instrument. Among the CV candidates in ω Cen (though not in NGC 6397), there is a trend toward higher f_X/f_R ratios for fainter sources (e.g., median $f_X/f_R = 2.8$ for sources with $M_{625} < 10$ vs. 6.8 for sources with $M_{625} > 10$). If a similar trend were present among 47 Tuc CVs, then the fact that only relatively bright CVs are present in the sample could account for at least part of the difference. Interestingly, Edmonds et al. (2003b) show that even the 47 Tuc CVs have higher f_X/f_{opt} ratios than field CVs reported by Verbunt et al. (1997), and a combination of X-ray luminosities and optical fluxes that are hard to reconcile with any known class of field CV. These comparisons should be interpreted with caution, however, given the difficulty of intercomparing CV samples collected using a wide variety of discovery methods (see Knigge [2011] for a discussion).

While the number of CV candidates in ω Cen is among the largest yet observed in a globular cluster, it is nevertheless quite small in comparison to the enormous mass of the cluster, which is estimated at $4 \times 10^6 M_\odot$ (Pryor & Meylan 1993). Considering that the ACS/WFC mosaic extends just beyond the half-mass radius, 27 CVs implies $\sim 1.4 \times 10^{-5}$ CVs per solar mass in ω Cen. For comparison, the space density of CVs in the solar neighborhood is $\sim 10^{-5} \text{ pc}^{-3}$ (Patterson 1998; Pretorius et al. 2007), or $10^{-4} M_\odot^{-1}$ considering the local mass density of $\sim 0.1 M_\odot \text{ pc}^{-3}$. Even if the current census of CVs represents only half of the true population (e.g., due to the current X-ray detection limit and/or crowding precluding the recovery of at least some optical counterparts), the frequency of CVs per unit mass in ω Cen would still be a factor of $\gtrsim 3$ lower than in the field. While the space density of CVs is uncertain, this result suggests that, to the extent that globular clusters both destroy CVs (and their progenitors) and create them (Davies 1997, Ivanova et al. 2006, Pooley & Hut 2006), destruction may be the dominant process in ω Cen.

The opposite is likely to be true of NGC 6397. Pooley & Hut (2006) have shown that dynamical processes dominate the production of CVs in dense clusters like NGC 6397. A comparison of the numbers of CV candidates in NGC 6397 vs. ω Cen (counting only CVs bright enough to have been detected in both X-rays and optical in either cluster) shows that NGC 6397 contains nearly 7 times more CVs per unit mass than ω Cen (which is ~ 16 times more massive than NGC 6397; Pryor & Meylan 1993). This finding further supports the view that NGC 6397 is able to generate new CVs by dynamical processes.

The contrast in formation histories of the CVs in the two clusters may help to explain one notable difference between the two samples. While the numbers of the most luminous CVs are similar in both clusters (e.g., 5 each in the decade between $L_x = 2 \times 10^{31} - 2 \times 10^{32} \text{ erg s}^{-1}$), ω Cen contains a factor of ~ 3 more faint CV candidates

in the decade from $L_x = 10^{30} - 10^{31}$ erg s^{-1} (see Fig. 5). This is despite what is likely to be a lower rate of recovery of faint optical counterparts in ω Cen due to crowding (1.7 million stars in 9 WFC pointings in ω Cen [Anderson & van der Marel 2010] vs. 25,000 in NGC 6397 in one WFC pointing [Strickler et al. 2009]). Since CVs evolve toward fainter luminosities as they age (e.g., Patterson 1984; Townsley & Gänsicke 2009; Knigge, Baraffe, & Patterson 2011), the larger proportion of faint CVs in ω Cen could be indicative of a population that is older on average. In qualitative terms at least, this is just as might be expected if ω Cen’s population is dominated by CVs of primordial origin while CVs in NGC 6397 have been produced in dynamical interactions over much of its lifetime.

4.2. Active binaries on or near the anomalous RGB/SGB

An unexpected result of our search for optical counterparts of X-ray sources in and toward ω Cen is the discovery of a population that appears to be associated with the anomalous giant and subgiant branches in the cluster (see §3.4). The X-ray luminosities of these stars are in the range $\sim 2 - 40 \times 10^{30}$ erg s^{-1} , which is significantly higher than would be expected for a population of old single stars. It is however characteristic of RS CVn-type binary stars, in which a giant or subgiant star is rotating fast as a result of tidal locking with a binary companion in a few-day orbit (Dempsey et al. 1993). The soft X-ray colors of these stars (see Fig. 5) are also typical of such coronal sources (cf. Heinke et al. 2005). Spectra are needed to determine whether these stars have the radial-velocity variability characteristic of such binaries, and whether their metallicities make them members of the anomalous RGB/SGB population in the cluster. In the meantime, given the X-ray evidence, we assume that they are indeed binaries, and consider the implications if they are (or are not) RGB/SGB-a members.

If these stars are members of the anomalous giant and subgiant populations in ω Cen, it would suggest that this relatively metal-rich population is somehow able to produce binaries much more efficiently (by a factor of 5 to 15—see §3.4) than the intermediate and low-metallicity populations that dominate the cluster. Alternatively, the binary fraction could be similar among the different populations if the binaries in the anomalous RGB/SGB-a population were on average more luminous in X-rays (e.g., as a result of increased coronal activity), such that a larger fraction were above the *Chandra* detection limit. The anomalous RGB/SGB-a population in ω Cen (whose corresponding main sequence has now also been identified—see Bellini et al. 2010) is a factor of ~ 10 more rich in metals than the dominant population in the cluster ($[Fe/H] \simeq -0.6$ to -0.8 vs. $[Fe/H] = -1.7$; Sollima et al. 2005, Johnson & Pilachowski 2010). It is thought to be the last in a series of discrete star formation episodes early in the life of ω Cen, producing increasingly high metal abundances as a result of self-enrichment. A factor of ~ 5 – 15 enhancement in the binary fraction in this population would be surprising considering that the frequency of field binaries shows no dependence on metallicity (Latham et al. 2002, Carney et al. 2005). On the other hand, metallicity is known to have a significant effect on the frequency of another class of binaries in glob-

ular clusters: LMXBs are three times more likely to be found in metal-rich clusters than in metal-poor clusters (Grindlay 1993, Bellazzini et al. 1995). While the cause for this difference is still debated (see Ivanova et al. 2006 and references therein), a second case of enhanced binary fraction in a metal-rich cluster population would be quite interesting. We note that recent theoretical work by Vesperini et al. (2011) suggests that significant differences could exist between the binary star populations in first-generation vs. second-generation stars in globular clusters with multiple stellar populations. However, their study finds an opposite effect to what is observed here (assuming these stars are members of the anomalous population), with binaries being more abundant among the first generation of stars.

If the metallicities of these stars reveal instead that they are members either of the metal-poor population or one of the intermediate-metallicity populations in ω Cen (Sollima et al. 2005), then their location in the CMD carries a different significance. In this case they would add to a growing number of globular and open clusters in which small number of red stragglers have been found (e.g., Belloni et al. 1998, Albrow et al. 2001, Kaluzny 2003, Edmonds et al. 2003a, Bassa et al. 2004, Bassa et al. 2008, Geller et al. 2008, Huang et al. 2010, Cohn et al. 2010, Platais et al. 2011). Red stragglers are loosely defined to be stars that lie redward of the turnoff. Typically they appear below the subgiant branch, but there are exceptions to this (see below). The term was coined by Albrow et al. (2001) to describe a group of six variable stars that appeared on the red side of the main-sequence turnoff in their HST/WFPC2 study of 47 Tuc. Five of these are likely BY Dra-type binary stars with periods in the range 4.9–9.2 days; the sixth is a CV. Three additional red stragglers were identified by Edmonds et al. (2003a) as optical counterparts of *Chandra* sources. All but one of the red stragglers in 47 Tuc have *Chandra* counterparts (Edmonds et al. 2003a, Heinke et al. 2005). Like the stars in question in ω Cen, the X-ray luminosities and soft X-ray colors of these stars (with the exception of the known CV) are indicative of coronal sources, consistent with their being binaries containing chromospherically active stars.

Red stragglers are particularly intriguing because they cannot be explained by the simple superposition of two normal stars. In general, some sort of mass transfer, which can take a star out of thermal equilibrium at least temporarily, has been invoked to make sense of them. The most detailed study to date of stars redward of the turnoff is that of two stars that appear below the subgiant branch in the old open cluster M67 (Mathieu et al. 2003). Proper motions and radial velocities both point to their being probable cluster members. Dubbed “sub-subgiants” by Belloni et al. (1998), spectroscopic analyses reveal that both are binaries, with periods of 2.8 and 18.4 days, respectively, and have the strong Ca II H and K emission line cores characteristic of coronal sources as well as H α in emission (Pasquini & Belloni 1998, van den Berg et al. 1999). Their X-ray luminosities are also typical of such systems (Belloni et al. 1998). Mathieu et al. (2003) conduct an exhaustive analysis of all available data and conclude that it is likely that both binaries have experienced mass transfer and/or significant dynamical interactions with other stars (see also Hurley et al. 2001),

but are unable to fully explain their locations ~ 1 magnitude below the subgiant branch. Clearly there is more to be learned from these enigmatic stars.

One important step will be to obtain more complete and unbiased samples than currently exist. Until recently nearly all red stragglers known in globular clusters were identified either as counterparts to X-ray sources or as photometric variables. Both of these detection methods are strongly biased toward finding binaries. They are also likely to select only the more extreme members of a larger class. Even the region in the CMD that such stars can occupy is unclear at present. For example, while the terms “red straggler” and “sub-subgiant” have generally been considered interchangeable, it appears that not all such stars that arguably belong in this class are fainter than subgiants. In the open cluster NGC 188, two cluster members (one of which has been shown to be binary) are adjacent to the base of the red giant branch (Geller et al. 2008). In ω Cen, two or three of the red straggler candidates we identify here are also brighter than subgiants (depending on which population of subgiants is chosen as a reference).

Proper motion measurements can ameliorate this situation by providing unbiased samples in globular clusters, as has been done for open clusters. The recent study of red stragglers in ω Cen that makes use of ground-based proper motions measurements by Bellini et al. (2009) is instructive. Rozycka et al. (2012) identify 13 red stragglers in ω Cen (the largest number yet uncovered in any study), all of which have colors significantly redder even than the RGB/SGB-a sequences in the cluster (and one of which is brighter than the subgiant branch). In the absence of both proper motion and radial velocity measurements suggesting otherwise, these stars would likely have been dismissed as unrelated to the cluster. Interestingly, Rozycka et al. (2012) find evidence that well over half are binaries, and surmise that they all may be. Given the extreme that ω Cen represents among globular clusters in many regards (including the recent and surprising discovery of a population of faint and very red main-sequence stars; King et al. 2012), it remains to be seen whether such extreme red stragglers are commonplace in globulars.

In comparing red stragglers in globular clusters vs. open clusters, it is notable that the numbers seen in globulars are not in general much greater than the numbers seen in open clusters, despite the vastly different total numbers of stars they contain. In ω Cen, with an estimated mass of $3 \times 10^6 \mathcal{M}_{\odot}$, 20 are now known. Scaling these numbers to M67, whose mass is more than 3 orders of magnitude lower (Fan et al. 1996), one would not expect to find any such stars. Yet two are known. NGC 6791, an open cluster with eight known red stragglers (Kaluzny 2003, Platais et al. 2011), is an even more extreme example. Despite the incompleteness of the current samples, it seems very likely that open clusters have a significantly higher specific frequency of red stragglers than globular clusters.

4.3. Where are the main-sequence binaries?

By comparison to the large numbers of CV candidates we have identified among the *Chandra* sources, the numbers of potential main-sequence binaries in the form of BY Dra stars is very small. This is in stark contrast to

the situation in NGC 6397, in which a search using the same camera and filters on *HST* revealed nearly three times as many active binaries as CVs (42 vs. 15; Cohn et al. 2010). A smaller yield is to be expected in ω Cen due to a higher degree of crowding and its larger distance (making the limit of the present search ~ 1.5 magnitudes brighter than in NGC 6397). Taking these factors into account, we estimate that ~ 10 of the NGC 6397 ABs, if present in ω Cen, should have been detectable in our optical data. Finding only 3 BY Dra stars is even more surprising in view of the fact that ω Cen is a factor of ~ 40 times more massive than NGC 6397 (Harris 1996), and that the present mosaic encompasses ~ 1.7 million measured stars (vs. $\sim 25,000$ in the NGC 6397 dataset). If the two clusters harbor similar fractions of close MS binaries one might have expected hundreds of ABs in ω Cen.

The critical difference between the two searches is not the optical data, but the X-ray data. Whereas the limiting X-ray luminosity in the existing ω Cen imaging is $L_x \sim 10^{30}$ erg s $^{-1}$, the limit is $\lesssim 10^{29}$ erg s $^{-1}$ in NGC 6397—more than an order of magnitude lower. Nevertheless, if ω Cen does harbor as large a population of BY Dra stars as NGC 6397 (per unit mass), it is still surprising to have found so few, considering that Dempsey et al. (1997) find that about 15% of field BY Dra binaries have $L_x > 10^{30}$ erg s $^{-1}$ (see their Fig. 4). On the other hand, of the > 30 ABs in NGC 6397 that lie in the part of the CMD associated with main-sequence binaries, not a single one is bright enough in X-rays to have been detected in the ω Cen *Chandra* imaging (see Fig. 6 of Cohn et al. 2010). This is interesting in itself, as it suggests that there may be significant differences between the populations of short-period MS binaries in globular clusters vs. the field. Deeper *Chandra* imaging is clearly needed to determine whether there are significant differences between the short-period MS binary populations in ω Cen vs. NGC 6397.

5. SUMMARY AND CONCLUSIONS

We have used ACS/WFC to identify optical counterparts for 59 *Chandra* sources in and toward Omega Centauri. Among the sources likely to be associated with the cluster are 27 candidate cataclysmic variables, a blue straggler, a qLMXB, and three possible BY Draconis-type binaries. In addition, we find 7 giants and subgiants whose locations in a color–magnitude diagram suggest either that they are red stragglers or that they are members of the most metal-rich RGB/SGB population in the cluster.

The frequency of CVs in ω Cen appears to be lower than the frequency of CVs in the Galactic field, by a factor of ~ 3 if we assume that half of ω Cen CVs have yet to be discovered. This suggests that the majority of binaries that would give rise to CVs in the field are destroyed in the cluster environment. Alternatively, the primordial binary fraction in ω Cen may have been lower than that in the field. We have also compared the properties of the CVs in ω Cen to the CVs in NGC 6397. Both are X-ray-selected samples, with optical IDs obtained using the same method. CVs are 7 times more frequent per unit mass in NGC 6397 than in ω Cen, and are likely to have been formed primarily through dynamical interactions. We find no measurable difference in the distribution of

X-ray-to-optical flux ratios for CVs in the two clusters. To the extent that X-ray-to-optical flux ratios are indicators of CV subtype, we find no indication that the types of CVs present in the two clusters differ, despite their contrasting formation histories.

Globular clusters have the potential to test CV evolutionary theory by providing samples of CVs all at the same relatively well-known distance—albeit with the added complication of cluster dynamics. Among the CVs in ω Cen is a faint group with absolute magnitudes similar to those of field CVs identified in the Sloan Digital Sky Survey, whose orbital periods are near the theoretical minimum for CVs (Gänsicke et al. 2009). A similarly faint population of CVs was identified in NGC 6397 by Cohn et al. (2010). Thus, both clusters for which sufficiently sensitive observations have been made are found to contain significant numbers of these faint systems. This provides qualitative evidence in support of the theory, which predicts a pile up of old, faint CVs near the period minimum. However, orbital periods are needed before more definitive conclusions can be drawn. Meaningful CV luminosity functions will also require determining the extent to which existing samples are incomplete due to the effects of crowding in optical imaging. In the case of ω Cen, deeper X-ray observations are also needed to sample the faintest systems.

One notable difference between the CV populations now known in ω Cen vs. NGC 6397 is the relative numbers of bright vs. faint CVs. The proportion of faint systems is a factor of ~ 2 -3 times higher in ω Cen than in NGC 6397, which suggests that the CVs in ω Cen may be older on average than those in NGC 6397. This supports the view that ω Cen's population is dominated by CVs that derive from primordial binaries, while NGC 6397 is continually manufacturing new compact binaries through dynamical interactions.

While nearly 50% of the optical counterparts we have identified appear to be compact binaries, only about 5% have characteristics indicative of BY Dra stars. This is in contrast to NGC 6397, in which active main-sequence binaries outnumber CVs by almost three to one (Cohn et al. 2010). These faint X-ray sources provide a valuable window into populations of short-period main-sequence binaries in globular clusters. Deeper *Chandra* imaging of ω Cen is needed to determine whether there are real differences between the relative numbers of these two classes of binaries in the cluster. The paucity of BY Dra candidates in the present study may simply be a consequence of the $\sim 10^{30}$ erg s $^{-1}$ limiting luminosity of the existing *Chandra* study (HCD09).

Seven of the optical counterparts have magnitudes and colors that place them on or near the anomalous giant and subgiant branches in ω Cen. The X-ray properties of these stars suggest that they may be RS CVn-type binaries. If the apparent association between these stars and the RGB/SGB-a stars is real, then the frequency of binaries in this metal-rich population is enhanced by a factor of five relative to the other giant and subgiant populations in the cluster. Spectroscopic observations are needed to determine whether or not these stars have metallicities that indicate membership in the RGB/SGB-a population.

If these stars are not members of ω Cen's most metal-rich population, then they lie in a region of the CMD

that cannot be explained by single-star evolution. In this case, they add to a growing number of red stragglers that have been identified in ω Cen, making it the cluster with the largest such population yet known.

We gratefully acknowledge discussions with Craig Heinke, Aaron Geller, Haldan Cohn and Phyllis Lugger, and thank the anonymous referee for helpful comments that improved the manuscript. This work is based on observations with the NASA/ESA Hubble Space Telescope and was supported by NASA grant HST-GO-9442 from the Space Telescope Science Institute, which is operated by the Association of Universities for Research in Astronomy, Incorporated, under NASA contract NAS5-26555. Support was also provided by Chandra Award Number GO0-1040A issued by the Chandra X-ray Observatory Center, which is operated by the Smithsonian Astrophysical Observatory for and on behalf of the National Aeronautics Space Administration under contract NAS8-03060.

REFERENCES

- Agüeros, M. A. et al. 2009, ApJS, 181, 444
 Albrow, M. D., Gilliland, R. L., Brown, T. M., Edmonds, P. D., Guhathakurta, P., & Sarajedini, A. 2001, ApJ, 559, 1060
 Anderson, J. 1997, Ph.D. thesis, UC, Berkeley
 Anderson, J. 2002a, in ASP Conf. Ser. 265, Omega Centauri, A Unique Window into Astrophysics, ed. F. van Leeuwen, J. D. Hughes, & G. Piotto (San Francisco: ASP), 87
 Anderson, J. 2002b, in Proceedings of the 2002 HST Calibration Workshop, ed. S. Arribas, A. Koekemoer, & B. Whitmore
 Anderson, J. 2003, in ASP Conf. Ser. 296, New Horizons in Globular Cluster Astronomy, ed. G. Piotto, G. Meylan, S. G. Djorgovski, & M. Riello (San Francisco: ASP), 125
 Anderson, J., Cool, A. M., & King, I. R. 2003, ApJ, 597, L137
 Anderson, J., & van der Marel, R. P. 2010, ApJ, 710, 1032
 Bailyn, C. D., Rubenstein, E. P., Slavin, S. D., Cohn, H. N., Lugger, P. M., Cool, A. M., & Grindlay, J. E. 1996, ApJ, 473, L31
 Bassa, C. et al. 2004, ApJ, 609, 755
 Bassa, C. G., Pooley, D., Verbunt, F., Homer, L., Anderson, S. F., & Lewin, W. H. G. 2008, A&A, 488, 921
 Bedin, L. R. et al. 2005, MNRAS, 357, 1038
 Bedin, L. R., Piotto, G., Anderson, J., Cassisi, S., King, I. R., Momany, Y., & Carraro, G. 2004, ApJ, 605, L125
 Bekki, K., & Freeman, K. C. 2003, MNRAS, 346, L11
 Bellazzini, M., Pasquali, A., Federici, L., Ferraro, F. R., & Fusi Pecci, F. 1995, ApJ, 439, 687
 Bellini, A. et al. 2009, A&A, 493, 959
 Bellini, A., Bedin, L. R., Piotto, G., Milone, A. P., Marino, A. F., & Villanova, S. 2010, AJ, 140, 631
 Belloni, T., Verbunt, F., & Mathieu, R. D. 1998, A&A, 339, 431
 Bogdanov, S., van den Berg, M., Heinke, C. O., Cohn, H. N., Lugger, P. M., & Grindlay, J. E. 2010, ApJ, 709, 241
 Brown, E. F., Bildsten, L., & Rutledge, R. E. 1998, ApJ, 504, L95
 Cannon, R. D., & Stobie, R. S. 1973, MNRAS, 162, 207
 Carney, B. W., Aguilar, L. A., Latham, D. W., & Laird, J. B. 2005, AJ, 129, 1886
 Carson, J. E., Cool, A. M., & Grindlay, J. E. 2000, ApJ, 532, 461
 Chevalier, C., & Ilovaisky, S. 1997, A&A, 326, 228
 Clark, G. W. 1975, ApJ, 199, L143
 Cool, A. M., Grindlay, J. E., Bailyn, C. D., Callanan, P. J., & Hertz, P. 1995a, ApJ, 438, 719
 Cool, A. M., Grindlay, J. E., Cohn, H. N., Lugger, P. M., & Bailyn, C. D. 1998, ApJ, 508, L75
 Cool, A. M., Grindlay, J. E., Cohn, H. N., Lugger, P. M., & Slavin, S. D. 1995b, ApJ, 439, 695
 Cohn, H. N. et al. 2010, ApJ, 722, 20
 Davies, M. B. 1997, MNRAS, 288, 117
 Dempsey, R. C., Linsky, J. L., Fleming, T. A., & Schmitt, J. H. M. M. 1993, ApJS, 86, 599

- Dempsey, R. C., Linsky, J. L., Fleming, T. A., & Schmitt, J. H. M. M. 1997, *ApJ*, 478, 358
- D’Ercole, A., Vesperini, E., D’Antona, F., McMillan, S. L. W., & Recchi, S. 2008, *MNRAS*, 391, 825
- Di Stefano R., & Rappaport, S. 1994, *ApJ*, 423, 274
- Djorgovski, S. 1993, in *ASP Conf. Ser. 50, Structure and Dynamics of Globular Clusters*, ed. S. G. Djorgovski & G. Meylan (San Francisco: ASP), 373
- Edmonds, P. D., Gilliland, R. L., Heinke, C. O., & Grindlay, J. E. 2003a, *ApJ*, 596, 1177
- Edmonds, P. D., Gilliland, R. L., Heinke, C. O., & Grindlay, J. E. 2003b, *ApJ*, 596, 1197
- Edmonds, P. D., Gilliland, R. L., Heinke, C. O., Grindlay, J. E., & Camilo, F. 2001, *ApJ*, 557, L57
- Fan, X. et al. 1996, *AJ*, 112, 628
- Feigelson, E. D. et al. 2002, *ApJ*, 574, 258
- Ferraro, F. R., Sollima, A., Pancino, E., Bellazzini, M., Straniero, O., Origlia, L., & Cool, A. M. 2004, *ApJ*, 603, L81
- Freeman, K. C., & Rodgers, A. W. 1975, *ApJ*, 201, L71
- Gänsicke, B. T. et al. 2009, *MNRAS*, 397, 2170
- Geller, A. M., Mathieu, R. D., Harris, H. C. & McClure, R. D. 2008, *AJ*, 135, 2264
- Gendre, B., Barret, D., & Webb, N. A. 2003, *A&A*, 400, 521
- Giacconi, R. et al. 1974, *ApJS*, 27, 37
- Grindlay, J. E. 1993, in *ASP Conf. Ser. 48, The Globular Cluster–Galaxy Connection*, ed. G. M. Smith & J. P. Brodie (San Francisco: ASP), 156
- Grindlay, J. E., Camilo, F., Heinke, C. O., Edmonds, P. D., Cohn, H., & Lugger, P. 2002, *ApJ*, 581, 470
- Grindlay, J. E., Cool, A. M., Callanan, P. J., Bailyn, C. D., Cohn, H. N., & Lugger, P. M. 1995, *ApJ*, 455, L47
- Güdel, M. 2004, *A&ARv*, 12, 71
- Haggard et al. 2004, *ApJ*, 613, 512
- Haggard, D., Cool, A. M., Arias, T., Brochmann, M. B., Anderson, J., & Davies, M. B. 2010, *AIP Conf. Proc.* 1314, 157
- Haggard, D., Cool, A. M., & Davies, M. B. 2009, *ApJ*, 697 224 (HCD09)
- Harris, W. E. 1996, *AJ*, 112, 1487
- Heinke, C. O. et al. 2005, *ApJ*, 625, 796
- Heinke, C. O., Ruiter, A. J., Muno, M. P., & Belczynski, K. 2008, in *AIP Conf. Proc. 1010, A Population Explosion: The Nature & Evolution of X-ray Binaries in Diverse Environments*, ed. R. M. Bandyopadhyay, S. Wachter, D. Gelino, & C. R. Gelino (Melville, NY: AIP), 136
- Hertz, P., & Grindlay, J. E. 1983a, *ApJ*, 267, L83
- Hertz, P., & Grindlay, J. E. 1983b, *ApJ*, 275, 105
- Huang, R. H. H., Becker, W., Edmonds, P. D., Elsner, R. F., Heinke, C. O., & Hsieh, B. C. 2010, *A&A*, 513, A16
- Hurley, J. R., Tout, C. A., Aarseth, S. J., & Pols, O. R. 2001, *MNRAS*, 323, 630
- Hut, P. et al. 1992, *PASP*, 104, 981
- Ivanova, N., Heinke, C. O., Rasio, F. A., Taam, R. E., Belczynski, K., & Fregeau, J. 2006, *MNRAS*, 372, 1043
- Johnson, C. I., & Pilachowski, C. A. 2010, *ApJ*, 722, 1373
- Kaluzny, J. 2003, *Acta Astronomica*, 53, 51
- Kaluzny, J., Kubiak, M., Szymanski, M., Udalski, A., Krzeminski, W., & Mateo, M. 1996, *A&ASupp.*, 120, 139
- King, I. R. et al. 2012, *AJ*, 144, 5
- Knigge, C. 2011, *Proc. Workshop on The Golden Age of Cataclysmic Variables and Related Objects*, ed. F. Giovanelli & L. Sabau-Graziati, at press (arXiv:1112.1074)
- Knigge, C., Baraffe, I., & Patterson, J. 2011, *ApJS*, 194, 28
- Knigge, C., Gilliland, R. L., Dieball, A., Zurek, D. R., Shara, M. M., & Long, K. S. 2006, *ApJ*, 641, 281
- Latham, D. W. et al. 2002, *AJ*, 124, 1144
- Lee, Y. W., Joo, J. M., Sohn, Y. J., Rey, S. C., Lee, H. C., & Walker, A. R. 1999, *Nature*, 402, 55
- Mathieu, R. D., van den Berg, M., Torres, G., Latham, D., Verbunt, V., & Stassun, K. 2003, *ApJ*, 125, 246
- Meylan, G. 2002, in *ASP Conf. Ser. 265, Omega Centauri, A Unique Window into Astrophysics*, ed. F. van Leeuwen, J. D. Hughes, & G. Piotto (San Francisco: ASP), 3
- Monelli, M. et al. 2005, *ApJ*, 621, L117
- Norris, J. E. 2004, *ApJ*, 612, L25
- Norris, J. E., & Da Costa, G. S. 1995, *ApJ*, 447, 680
- Norris, J. E., Freeman, K. C., & Mighell, K. J. 1996, *ApJ*, 462, 241
- Pancino, E., Ferraro, F. R., Bellazzini, M., Piotto, G., & Zoccali, M. 2000, *ApJ*, 534, L83
- Pasquini, L., & Belloni, T. 1998, *A&A*, 336, 902
- Patterson, J. 1984, *ApJS*, 54, 443
- Patterson, J. 1998, *PASP*, 110, 1132
- Piotto, G., et al. 2005, *ApJ*, 621, 777
- Platais, I., Cudworth, K. M., Kozhurina-Platais, V., McLaughlin, D. E., Meibom, S. & Veillet, C. 2011, *ApJ*, 733, L1
- Pooley, D. et al. 2002, *ApJ*, 569, 405
- Pooley, D. & Hut, P. 2006, *ApJ*, 646, L143
- Pretorius, M. L., Knigge, C., O’Donoghue, D., Henry, J. P., Gioia, I. M., & Mullis, C. R. 2007, *MNRAS*, 382, 1279
- Pryor, C., & Meylan, G. 1993, in *Structure and Dynamics of Globular Clusters*, ed. S. G. Djorgovski & G. Meylan (ASP Conf. Ser. 50), 357
- Renzini, A. 2008, *MNRAS*, 391, 354
- Riaz, B., Gizis, J. E., & Harvin, J. 2006, *AJ*, 132, 866
- Rozyczka, M., Kaluzny, J., Pietrukowicz, P., Pych, W., Catelan, M., & Contreras, C. 2012, *A&A*, 537, A89
- Rutledge, R. E., Bildsten, L., Brown, E. F., Pavlov, G. G., & Zavlin, V. E. 2000, *ApJ*, 529, 985
- Rutledge, R. E., Bildsten, L., Brown, E. F., Pavlov, G. G., & Zavlin, V. E. 2002, *ApJ*, 578, 405
- Sirianni, M. et al. 2005, *PASP*, 117, 1049
- Sollima, A., Pancino, E., Ferraro, F. R., Bellazzini, M., Straniero, O., & Pasquini, L. 2005, *ApJ*, 634, 332
- Stauffer, J. R., Caillault, J.-P., Gagné, M., Prosser, C. F., & Hartmann, L. W. 1994, *ApJS*, 91, 625
- Stetson, P. B. 1987, *PASP*, 99, 191
- Stetson, P. B. 1994, *PASP*, 106, 250
- Strickler, R. R., Cool, A. M., Anderson, J., Cohn, H. N., Lugger, P. M., & Serenelli, A. M. 2009, *ApJ*, 699, 40
- Suntzeff, N. B., & Kraft, R. P. 1996, *AJ*, 111, 1913
- Szkody, P. et al. 2011, *AJ*, 142, 181
- Taylor, J. M., Grindlay, J. E., Edmonds, P. D., & Cool, A. M. 2001, *ApJ*, 553, L169
- Townsley, D. M., & Bildsten, L. 2002, *ApJ*, 565, L35
- Townsley, D. M., & Gänsicke, B. T. 2009, *ApJ*, 693, 1007
- van den Berg, M., Verbunt, F., & Mathieu, R. D. 1999, *A&A*, 347, 866
- van Leeuwen, F., Hughes, J. D., & Piotto, G. 2002, *ASP Conf. Ser. 265, Omega Centauri, A Unique Window into Astrophysics* (San Francisco: ASP)
- van Leeuwen, F., Le Poole, R. S., Reijns, R. A., Freeman, K. C., & de Zeeuw, P. T. 2000, *A&A*, 360, 472
- Verbunt, F., & Johnston, H. M. 2000, *A&A*, 358, 910
- Verbunt, F., & Meylan, G. 1988, *A&A*, 203, 297
- Verbunt, F., van Paradijs, J., & Elson, R. 1984, *MNRAS*, 210, 899
- Verbunt, F., Bunk, W. H., Ritter, H., & Pfeffermann, E. 1997, *A&A*, 327, 602
- Vesperini, E., McMillan, S. L. W., D’Antona, F., & D’Ercole, A. 2011, *MNRAS*, 416, 355
- Villanova, S. et al. 2007, *ApJ*, 663, 296
- Young, A., Skumanich, A., Stauffer, J. R., Bopp, B. W., & Harlan, E. 1989, *ApJ*, 344, 427

Table 1
Candidate Optical Counterparts: Astrometry

X-ray ID ^a	Optical ^b ID#	x (pix)	y (pix)	offset ^c (pix)	quality ^d	type ^e	RA (J2000)	Dec (J2000)	cluster offset ^f (arcsec)
12a	1486	207.5	201.9	4.9	1	CV	13:26:48.651	-47:27:44.82	63
13a	9205	205.3	201.8	4.9	0	CV	13:26:53.513	-47:29:00.38	65
13b	1398	207.8	194.9	11.8	1	RGB/SGB-a	13:26:50.532	-47:29:18.15	46
13c	1408	206.4	200.8	5.8	1	CV	13:26:52.135	-47:29:35.63	69
13f	3001	205.0	201.8	4.9	1	CV?	13:26:45.980	-47:29:16.63	32
14a	8018	200.2	208.1	6.1	1	BYDra	13:26:45.770	-47:28:59.19	19
21b	8001	206.7	204.9	1.8	1	fbCV	13:26:35.341	-47:27:59.15	129
21c	9121	212.3	209.2	6.7	1	H α -only	13:26:36.888	-47:27:45.72	121
""	1310	212.4	203.9	6.9	1	H α -only	13:26:36.862	-47:27:45.75	121
21d	4017	206.7	213.7	7.1	1	H α -only	13:26:38.308	-47:27:40.36	112
""	1350	202.9	210.3	4.9	1	blue-only	13:26:38.292	-47:27:40.58	112
22a	1074	206.3	204.6	2.0	0	FGND	13:26:48.299	-47:26:41.21	125
22c	1347	206.3	207.9	1.3	0	fbCV	13:26:52.687	-47:27:13.41	108
22d	4003	205.7	201.3	5.3	1	BS	13:26:58.746	-47:27:28.93	140
22e	1340	204.2	202.1	4.9	1	RGB/SGB-a	13:26:59.926	-47:28:09.68	133
22f	1287	205.2	195.3	11.3	1	AGN	13:26:58.809	-47:28:21.19	119
""	1334	196.7	202.4	10.3	1	blue-only	13:26:58.847	-47:28:21.56	120
23b	1187	207.2	195.7	11.0	1	CV?	13:26:51.683	-47:30:47.33	128
""	1238	211.1	202.4	6.5	1	blue-only	13:26:51.714	-47:30:47.09	128
23c	5000036	211.5	197.7	10.4	1	AGN	13:26:48.051	-47:30:14.36	88
24a	1413	205.2	204.4	2.4	1	blue-only	13:26:44.466	-47:30:06.03	84
24c	1217	207.3	204.0	2.9	0	CV	13:26:38.417	-47:30:36.75	141
24e	1034	206.1	217.4	10.8	1	BYDra	13:26:36.852	-47:30:11.55	135
24f	5000592	201.7	209.7	5.4	1	RGB/SGB-a	13:26:37.287	-47:29:42.93	115
24g	6001	207.5	205.5	1.8	1	AGN?	13:26:34.387	-47:29:55.71	147
31a	7005	209.5	199.1	8.2	0	fbCV	13:26:29.356	-47:28:13.21	184
31b	9002	204.6	208.6	2.5	1	AGN	13:26:31.391	-47:28:01.53	166
32a	9001	209.1	207.8	3.2	0	fbCV	13:26:46.353	-47:25:18.45	208
32c	1082	207.1	210.1	3.6	1	H α -only	13:26:55.907	-47:26:02.18	186
32f	7003	203.8	201.5	5.6	1	RGB/SGB-a	13:27:05.331	-47:28:08.78	187
33c	1248	210.0	205.5	4.1	1	blue-only	13:27:03.620	-47:28:57.87	166
33d	1268	197.2	206.0	8.9	0	H α -only	13:27:01.461	-47:29:25.17	149
33e	1281	199.9	211.3	7.8	0	CV?	13:27:00.974	-47:30:04.72	159
""	3128	198.8	215.4	11.4	1	CV?	13:27:00.995	-47:30:04.75	159
33h	1110	207.3	195.9	10.8	1	blue-only	13:26:55.066	-47:31:13.69	167
33j	3001	199.0	213.0	9.6	0	fbCV	13:26:49.621	-47:31:24.83	160
33l	1117	207.1	200.8	5.9	1	AGN?	13:26:48.731	-47:31:25.28	159
33m	1112	214.3	207.0	8.2	1	CV?	13:26:46.491	-47:31:40.75	174
34b	1204	200.2	208.3	6.1	0	RGB/SGB-a	13:26:37.440	-47:30:53.34	161
41a	637	205.6	205.3	1.4	1	H α -only	13:26:24.423	-47:26:57.72	255
41d	930	207.8	201.6	5.3	1	CV	13:26:28.651	-47:26:27.29	234
41g	6005	203.3	212.6	6.6	1	AGN	13:26:37.460	-47:24:29.93	275
41h	915	208.3	218.3	11.9	0	RGB/SGB-a	13:26:43.958	-47:24:42.63	246
42c	1015	211.8	208.8	6.1	0	RGB/SGB-a	13:27:09.652	-47:27:28.85	240
43c	1347	205.6	200.0	6.6	1	RGB/SGB-a	13:27:06.910	-47:30:09.42	215
43e	1029	203.4	196.9	10.1	0	BYDra	13:27:03.426	-47:30:56.33	209
43f	2001	205.5	203.6	3.1	0	FGND	13:26:56.047	-47:32:02.16	215
43h	914	202.5	202.7	5.3	1	CV?	13:26:49.584	-47:32:12.83	207
44a	833	207.4	199.1	7.6	1	blue-only	13:26:44.102	-47:32:31.46	227
44c	7003	210.2	209.5	5.0	0	fbCV	13:26:23.641	-47:30:43.83	266
""	798	200.8	216.1	10.9	1	AGN?	13:26:23.678	-47:30:44.27	266
44d	896	209.9	204.6	4.3	0	CV?	13:26:22.858	-47:30:09.14	260
44e	788	206.3	207.4	0.8	0	qLMXB	13:26:19.796	-47:29:10.51	279
51a	5000018	214.7	207.2	8.6	1	blue-only	13:26:31.315	-47:24:39.27	295
51d	670	208.3	202.2	4.9	0	H α -only	13:26:40.994	-47:24:02.22	291
51e	823	207.1	215.3	8.8	1	FGND	13:26:44.764	-47:23:33.59	313
""	5000005	215.4	204.4	9.6	1	FGND	13:26:44.708	-47:23:33.24	314
52b	738	210.0	214.3	8.6	0	AGN	13:26:54.948	-47:24:08.88	288
""	748	207.3	217.9	11.4	0	AGN	13:26:54.967	-47:24:08.99	288
52c	521	201.4	209.1	5.3	0	AGN?	13:27:06.396	-47:25:38.20	270
52d	796	204.1	204.7	2.8	0	fbCV	13:27:14.923	-47:27:43.54	287
54b	5008	206.3	207.4	0.8	1	fbCV	13:26:42.452	-47:33:09.20	267
54d	617	206.2	207.7	1.1	0	AGN	13:26:25.127	-47:32:27.40	314
""	637	206.1	214.2	7.6	0	FGND	13:26:25.159	-47:32:27.35	314
54e	5006	202.5	203.9	4.5	1	fbCV	13:26:25.384	-47:31:40.97	281
54g	747	207.1	209.8	3.4	1	AGN	13:26:20.034	-47:30:15.18	289
""	715	212.9	200.3	9.3	1	H α -only	13:26:19.986	-47:30:14.97	290
54h	734	206.7	206.4	0.6	1	CV	13:26:20.366	-47:30:02.94	282
62b	538	202.2	212.8	7.3	0	AGN	13:27:08.011	-47:23:33.86	377

Note. — Astrometric properties of the candidate optical counterparts to the *Chandra* X-ray sources, sorted by X-ray ID (roughly the distance from the cluster center). ^aX-ray ID from HCD09. ^bOptical ID# from DAOPHOT (see §2.3). ^cOffset between the X-ray source and optical counterpart positions. The X-ray source position in physical coordinates is (x,y) = (206.1,206.6) in each patch after boresite correction (§2.1). The optical counterpart position in physical coordinates appears in the previous two columns. ^dEstimated quality of the photometry; 0=excellent, 1=good (see §2.3 for details). ^eAbbreviation for the most likely source classification: quiescent low mass X-ray binary (qLMXB), cataclysmic variable (CV), possible CV (CV?), faint blue CV (fbCV), BY Draconis-type binary (BYDra), blue straggler (BS), star located on or near anomalous subgiant or giant branch in CMD (RGB/SGB-a), H α -bright source with no measurable blue excess (H α -only), foreground star (FGND), background active galactic nucleus (AGN), possible AGN (AGN?), blue source with no measurable H α -excess (blue-only). Refer to Table 2 and §3 for photometric properties and a discussion of these classifications. ^fOffset between optical source position and cluster center, (RA,Dec) = (13:26:47.24,-47:28:46.45) from Anderson & van der Marel (2010).

Table 2
Candidate Optical Counterparts: Photometry

X-ray ID	R_{625} (mag)	$B_{435} - R_{625}$ (mag)	$H\alpha - R_{625}$ (mag)	color ^b	H α ^c	quality	type	f_X/f_R ^d	L_X ^e (10^{30} erg s ⁻¹)
44e	25.3	1.5	-1.2	blue	bright	0	qLMXB	440	120
13c	20.9	0.7	-0.5	blue	bright	1	CV	8.8	140
13a	20.0	1.1	-0.4	blue?	bright	0	CV	4.1	150
12a	21.3	1.0	-0.3	blue	bright	1	CV	4.2	48
54h	20.7	0.2	-0.1	blue	bright	1	CV	3.7	72
41d	22.2	1.3	-0.5	blue	bright	1	CV	5.0	24
24c	23.5	0.5	-1.0	blue	bright	0	CV	2.7	4.1
33e ^f	22.0	1.4	-0.2	blue	bright?	0	CV?	0.46	2.6
43h	22.6	0.5	-0.1	blue	bright?	1	CV?	3.7	12
33m	22.7	1.7	-0.4	blue?	bright	1	CV?	0.80	2.5
13f	24.2	1.0	-0.7	blue	bright?	1	CV?	3.5	2.7
23b ^f	24.5	0.7	-0.6	blue	bright?	1	CV?	4.1	2.4
44d	25.2	0.5	-1.0	blue	bright?	0	CV?	21	6.3
22c	24.5	1.0	...	blue	...	0	fbCV	22	13
31a	24.6	0.4	...	blue	...	0	fbCV	14	7.2
21b	24.8	0.0	...	blue	...	1	fbCV	3.1	1.4
52d	24.8	0.2	...	blue	...	0	fbCV	7.3	3.2
33j	24.9	-0.3	...	blue	...	0	fbCV	5.0	2.1
54b	25.2	1.4	...	blue	...	1	fbCV	20	6.2
54e	25.9	1.0	...	blue?	...	1	fbCV	5.8	1.0
32a	26.3	-0.4	...	blue	...	0	fbCV	24	2.6
44c ^f	26.3	0.2	...	blue	...	0	fbCV	30	3.3
24e	19.7	1.4	0.1	red?	bright?	1	BYDra	0.013	0.6
43e	20.3	1.5	0.1	red?	bright?	0	BYDra	0.055	1.5
14a	20.5	1.5	0.1	red?	bright?	1	BYDra	0.050	1.2
22d	17.0	0.9	-0.1	blue?	bright	1	BS	0.007	3.8
24f	15.5	1.5	0.1	red	neither	1	RGB/SGB-a	0.0007	1.6
22e	16.5	1.5	0.1	red	bright?	1	RGB/SGB-a	0.009	8.0
32f	16.8	1.5	0.1	red	bright?	1	RGB/SGB-a	0.006	4.0
13b	17.2	1.1	0.3	red	neither	1	RGB/SGB-a	0.010	4.9
43c	17.2	1.3	0.0	red	bright?	1	RGB/SGB-a	0.004	1.8
34b	17.5	1.3	-0.1	red	neither	0	RGB/SGB-a	0.075	28
42c	17.9	1.2	0.2	red	neither	0	RGB/SGB-a	0.005	1.4
41h	18.1	1.1	0.2	red	neither	0	RGB/SGB-a	0.006	1.4
21d ^f	21.1	1.7	-0.1	neither	bright?	1	H α -only	0.39	5.3
32c	21.1	1.6	0.0	neither	bright?	1	H α -only	0.18	2.4
33d	21.8	2.0	0.0	neither	bright?	0	H α -only	0.68	4.8
51d	22.9	2.3	-0.1	neither	bright?	0	H α -only	2.8	7.1
41a	24.5	2.5	-0.6	neither	bright?	1	H α -only	6.2	3.7
21c ^f	25.4	...	-0.9	...	bright?	1	H α -only	5.8	1.4
43f	17.7	2.0	0.0	red	bright	1	FGND	0.011	...
22a	19.6	2.5	-0.4	red	bright	0	FGND	0.021	...
51e ^f	19.8	2.1	-0.1	red	bright	1	FGND	0.056	...
52b ^f	20.9	0.8	0.4	blue	faint	0	AGN	0.068	...
22f ^f	21.6	2.3	0.2	red	faint?	1	AGN	0.57	...
54d ^f	22.2	0.7	0.3	blue	faint	0	AGN	8.8	...
31b	22.9	1.4	0.2	blue	neither	1	AGN	0.74	...
54g ^f	23.7	2.6	0.0	neither	neither	1	AGN	0.96	...
23c	23.8	...	0.4	...	faint?	1	AGN	2.6	...
62b	24.2	1.5	0.3	blue	faint?	0	AGN	18	...
41g	25.8	1.2	-0.9	blue?	bright?	1	AGN	39	...
52c	20.7	1.1	0.2	blue	faint	0	AGN?	0.58	...
33l	21.7	0.5	0.2	blue	faint	1	AGN?	3.4	...
24g	22.2	0.6	0.3	blue	faint	1	AGN?	2.2	...
33h	19.3	0.9	0.1	blue	neither	1	blue-only	0.20	...
44a	20.7	0.7	0.1	blue	neither	1	blue-only	2.2	...
51a	21.0	0.6	0.1	blue	neither	1	blue-only	0.78	...
33c	23.0	1.8	0.0	blue?	neither	1	blue-only	0.75	...
24a	23.8	2.1	0.0	blue?	neither	1	blue-only	1.5	...
Alternate Counterparts:									
33e	23.4	1.8	-0.4	blue?	bright	1	CV?	1.7	2.6
21c	24.8	...	-0.6	...	bright?	1	Ha-only	3.3	1.4
54g	25.2	...	-1.1	...	bright?	1	Ha-only	3.8	1.2
51e	15.9	1.7	0.1	red	bright?	1	FGND	0.002	...
54d	20.1	2.4	-0.2	red	bright	0	FGND	1.3	...
52b	21.3	0.6	0.3	blue	faint	0	AGN	0.096	...
44c	24.0	1.2	0.4	blue	faint	1	AGN?	3.5	...
21d	22.8	1.8	0.1	blue?	neither	1	blue-only	1.8	...
22f	23.6	1.7	-0.2	blue?	neither	1	blue-only	3.6	...
23b	23.3	1.8	0.3	blue?	neither	1	blue-only	1.4	...

Note. — Photometric properties of the candidate optical counterparts, sorted by source type. Within each type, the sources are listed in decreasing R_{625} -band brightness, except in the CV category where sources are listed as previously-known CVs first, then new CVs, then new CV?s. The quality index is described in §2.3. ^aX-ray ID from HCD09. ^bDescription of the candidate's location in the R_{625} vs. $B_{435} - R_{625}$ CMD (see Fig. 3 and §3 for details). ^cDescription of the candidate's location in the R_{625} vs. $H\alpha - R_{625}$ CMD (see Fig. 3 and §3 for details). ^dX-ray-to-optical flux ratio. Unabsorbed X-ray fluxes from HCD09, revised downward by a factor of 1.25; R_{625} -band fluxes assume $f_R = 10^{0.4R-5.89}$ (see §4.1). ^eX-ray luminosity calculated from the fluxes given by HCD09 assuming a distance of 4.9 kpc. ^fAlternate counterpart included in lower sub-table.